Chapter 2.2

Mechanics of the Cytoskeleton

2.2.1 Introduction

The cytoskeleton, the system of protein filaments that permeate the cytoplasmic space of all eukaryotic cells, is primarily responsible for the structural integrity exhibited by a cell and determines its deformation in response to a given stress. This fibrous matrix is instrumental to a wide variety of essential cell functions ranging from migration to adhesion to mitosis to mechanotransduction (the genetic response of a cell to mechanical stimuli). For some cells, their intrinsic elasticity determines their deformation in response to external forces. Cells such as those circulating within or lining the walls of the vascular system are subjected to fluid dynamic forces and change shape as a direct consequence of those forces. In other cells, such as those surrounded by a stiffer extracellular matrix, their shape is dictated by the deformation of the structures in which they are embedded and the cell's own elastic characteristics play little role in determining the magnitude of those deformations. Even in these, however, externally-imposed deformations produce intercellular forces that can influence cell secretions, gene expression and protein synthesis.

Cell migration results from an interaction between the forces of adhesion to structures external to the cell (extracellular matrix *in vivo* or cell culture substrate *for in vitro* preparations), and the cell's own intrinsic stiffness in response to internally generated forces. As will be shown in Chapter 2.3[1], the speed of migration depends on a critical balance between cell stiffness and adhesion strength such that migration speed is reduced when the cell is either too rigid or too compliant.

Mechanotransduction is the term used to describe gene expression in response to cellular deformations or forces acting on the cell. This appears to be a property of nearly all eukaryotic

[1] Note that the references to other chapters pertain to a book currently in-progress, most of which is not yet available to students.

cells and provides an important means by which the cells can respond to their environment. The response may be a protective one, leading for example to the formation of actin stress fibers within the cell or the production of new ECM materials to bolster stiffness of the surrounding network, or it may be a natural step in the sequence of development, leading to cell differentiation. Whatever the result, it is clear that cells are exquisitely sensitive to physical stresses present in their environment, a topic discussed in detail in Chapter 2.3.

While the importance of the cytoskeleton is well established, our understanding of the relationship between the microstructural details and the macroscopic properties they produce is still a matter of considerable debate and several fundamentally different models have been proposed. Part of the reason for this lack of consensus is that the cytoskeletal structure can appear quite distinct in different cell types. The stiffness exhibited by an erythrocyte, for example, as it deforms to pass through a narrow capillary is entirely different from that of an endothelial cell lining the vessel. Different molecular constituents may be responsible for the observed elasticity, and their structures differ markedly. Even in a single cell type, or a particular cell, the structure is highly variable and can change markedly in response to environmental factors such as mechanical or electrical stimulation.

This chapter starts by presenting what is known about the cytoskeletal microstructure, its configuration and molecular constituents in Section 2.2.2. Next, the various methods that have been used either to describe the elasticity of the matrix or to explain its physical basis are discussed in Section 2.2.3. In Section 2.2.4, we describe some of the experimental methods and results obtained that provide the basis for much of what we currently know about the cytoskeleton and its structural characteristics. Interpretation of the experimental results often requires some analysis and the methods used for this purpose are derived. These start from the most basic phenomenological models and proceed to the more recent microstructural descriptions. This matrix is immersed in a liquid, the cytosol, that influences primarily the dynamic response of the cell which, depending on the length scale of the measurement, can either appear as water or as a highly viscous or viscoelastic fluid (Section 2.2.5). Many of these concepts are subsequently applied in later chapters to understand the characteristics of particular cells types and to describe some of the differences that have been observed.

2.2.2 Constituents of the cytoskeleton

The cytoskeleton is the network of biopolymers that permeate the cell and give rise to its structural integrity. This network appears, on high magnification, to be comprised of several

distinct types of intertwined filaments with a variety of interconnections as can be seen in the micrograph of Fig. 1. The network, as seen at this high magnification, is not unlike that of other fibrous materials when viewed at much lower magnification (Fig. 2) and, as one might expect, shares some of the same structural characteristics. As with these other common materials, the apparent stiffness of the network depends fundamentally upon the elastic properties of the constituent fibers. For this reason, it is appropriate to begin this chapter by examining the biological composition and properties of the biopolymers that constitute the network. It is important to recognize, however, that unlike these other macroscale fibrous materials, the elastic properties of the cytoskeleton are also critically dependent upon the effects of thermal fluctuations as will be discussed later.

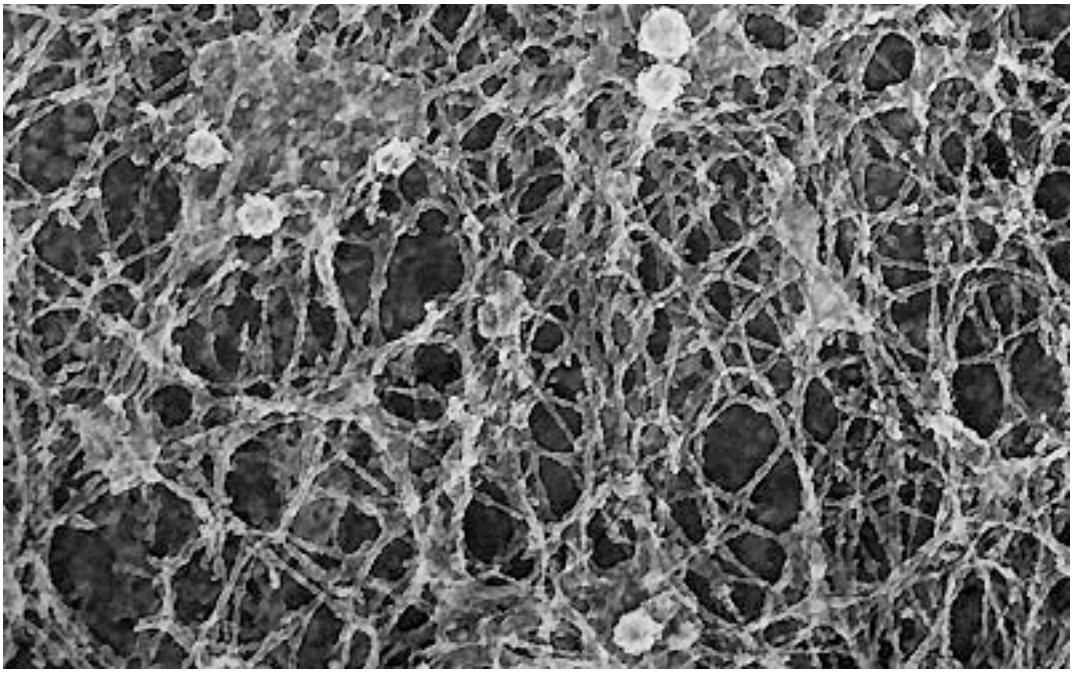

Fig. 1. The cytoskeleton of a macrophage lamellipodium as seen by electron microscopy. The fibrous structure is mainly comprised of actin filaments. (John Hartiwick)

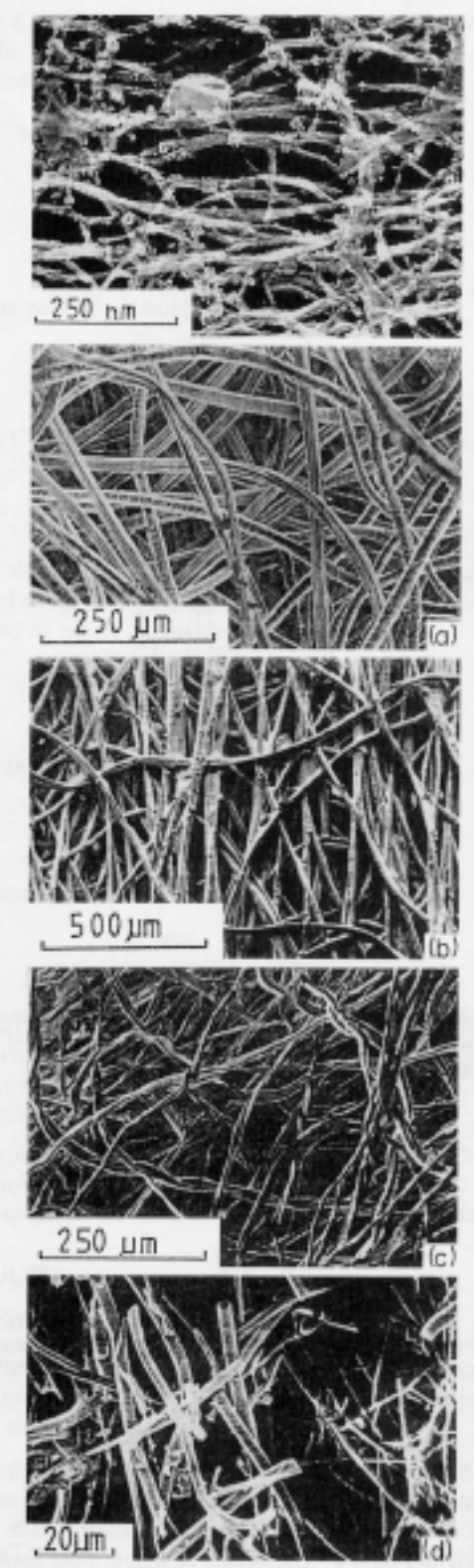

endothelial cell

felt

paper

cotton

space shuttle tile

Fig. 2. Comparison with other fibrous materials (from Gibson & Ashby)

The cytoskeletal matrix is primarily comprised of three constituents, actin microfilaments 7 to 9 nm in diameter, microtubules (24 nm), and intermediate filaments (~10 nm) (Table 4). These form a complex interconnected network that exists in a state of constant flux especially when the cell is dividing, migrating, or undergoing other dynamic processes. All are polymers built from protein subunits, held together by noncovalent bonds. They also share the common feature that they cross-link, often with the aid of other proteins, to form bundles and lattice networks. The secondary and tertiary structures formed by these polymers, as we will see, are critical determinants of cytoskeletal elasticity.

Actin microfilaments

Actin filaments play an essential role in virtually all types of motility. Actin-myosin interactions are of obvious importance in muscle, but are also instrumental in the migration and movement of non-muscle cells. Actin polymerization is thought to be one of the factors initiating cell migration through the formation of filopodia or lamellapodia [Svitkina & Borisy, 1999]. The actin matrix, though common to nearly all eukaryotes, may be organized differently in different cells. The fluorescent micrograph of Fig. 3 shows the organization of the filamentous actin (F-actin) in a migrating fibroblast cell. Notice the intense staining at the leading edge, and the large cable-like structures (stress fibers) aligned primarily in the direction of movement and connecting the rest of the cell to the protruding segment. Using a different preparation (freeze deep-etch, Fig. 4) the lattice structure typical of that in the cortical or cytoskeletal regions of resting cells, can be seen to be highly interconnected and relatively isotropic.

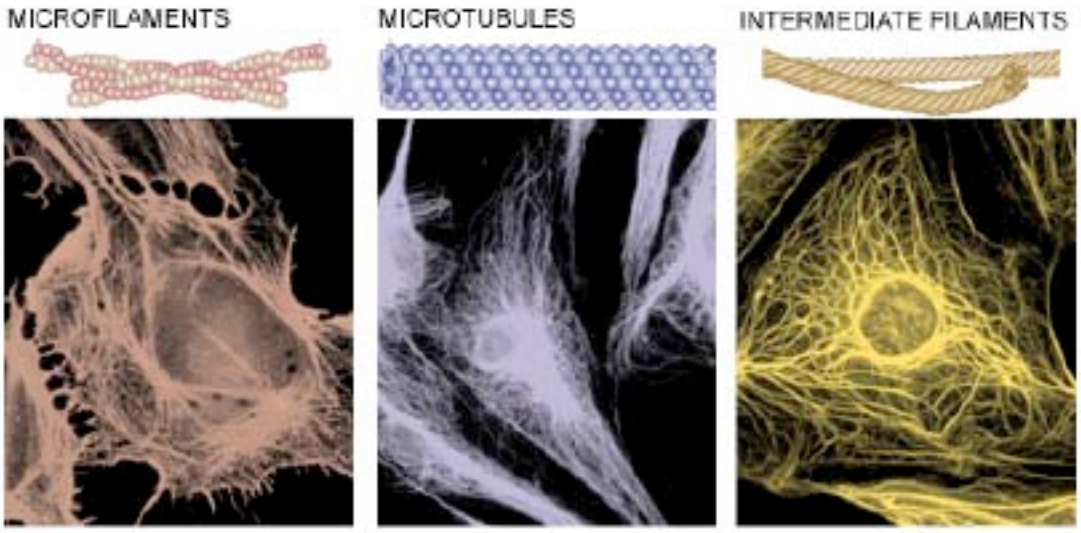

Fig. 3. Fluorescent micrographs showing actin microfilaments (left), microtubules (center) and intermediate filaments (right) (reproduced from Ingber, 1998).

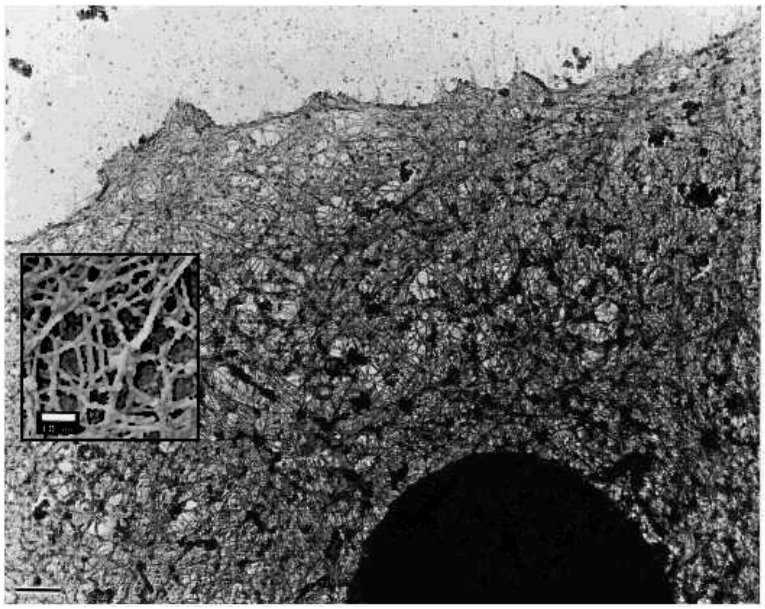

Fig. 4. Quick-freeze deep-etch image of the cytoskeleton of an endothelial cell (courtesy of J. Hartwick)

Actin is one of the most prevalent proteins found in the cell, ranging in concentration from 1 - 10% by weight of total cell protein in non-muscle cells, to 10-20% in muscle. Molecular actin is comprised of 375 residues (molecular weight 43 kDa), but is found in at least six forms that differ from each other only slightly. Of these, four are found in muscle, the other two in non-muscle cells. Actin exists either in globular form (G-actin monomers) or filamentous form (F-actin polymer) with the balance between the two being a highly dynamic process that is finely regulated by a variety of different factors. For example, the addition of certain ions (Mg^{2+}, K^{+}, Na^{+}) has been found to induce reversible polymerization of actin monomers. Cytochalasins, on the other hand, bind to the barbed ends of the actin filaments and prevent polymerization while phalloidin binds to the pointed ends and prevents dissociation into G-actin. F-actin assembly is regulated by capping proteins such as gelsolin that bind to barbed ends. Gelsolin also severs filaments, a process that can be activated by Ca^{2+}.

F-actin is a long, flexible filament about 7 nm in diameter. Subunits (monomers) are organized into a double-stranded helix having structural and functional polarity (pointed or negative, and barbed or positive ends) and a half-pitch of about 37 nm (Fig. 5). At the barbed end, an ATP binding cleft is exposed, allowing for binding of monomer and linear growth of the filament. ATP binding and hydrolysis play a critical role in regulating actin dynamics and

controlling the length of the actin filament. Within the cell, there exists a delicate balance between polymerization at the barbed ends and de-polymerization at the pointed ends.

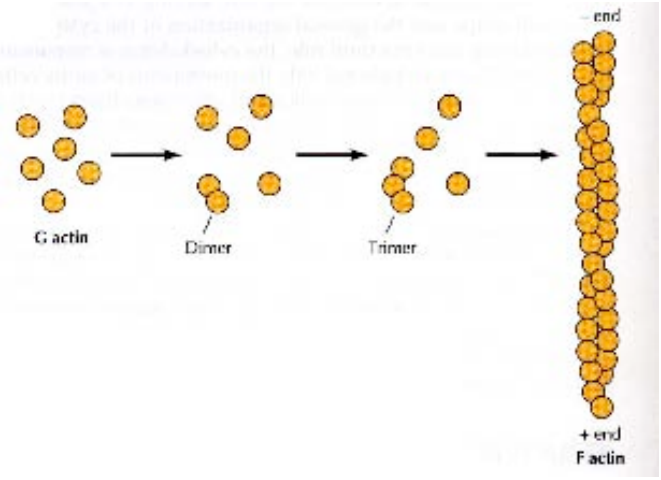

Fig. 5 Schematic showing the arrangement of G-actin monomers to form F-actin.

The F-actin filaments can further organize into tertiary structures such as bundles or a lattice network with the aid of *actin binding proteins* (ABP). The bundles, also referred to as *stress fibers*, are closely packed parallel arrays of filaments, connected to each other by several members of the ABP family (Table 1). These can vary in size, but are typically about 0.1 micron in diameter. Networks consist of an interconnected matrix of F-actin filaments, the junctions of which are often seen to be nearly orthogonal. At least two distinct types of network are observed - cortical (membrane-associated and more planar in nature) and non-membrane-associated which possess a more isotropic three-dimensional structure.

The formation of both bundles and networks is facilitated by a variety of cross-linking proteins, some of which are listed in Table 1. One in particular, ABP-280 or filamin (a dimer consisting of two 280 kDa subunits) forms a V-shaped polymer that connects two actin filaments nearly at right angles, forming a regular lattice in three dimensions. Others provide the connection of F-actin to the cell membrane.

The elastic properties of actin have been measured in a variety of ways: by axial stretch (Higuchi et al., 1995), twisting (Tsuda et al., 1996, Yasuda et al., 1996), and bending. By all methods, a single actin filament was found to exhibit a Young's modulus in the range of 1.3×10^9 N/m^2 to 2.5×10^9 N/m^2. This value compares favorably with those measured for silk and collagen (Gittes et al., 1993), and are also roughly consistent with predictions based on van der Waals bonding between surfaces (Howard, 2001).

Protein	Function	MW (kDa)	Location
thymosin	monomer binding	5	cytoskeleton
profilin	monomer binding, regulates barbed end	16	cytoskeleton
cofilin/ADF	monomer binding, regulates barbed end, filament severing	15-19	cytoskeleton
gelsolin	filament severing and capping protein	90	cytoskeleton
Arp2/3	filament capping, nucleation	44/50	cytoskeleton
fimbrin	filament cross-linking	68	microvilli, adhesion plaques
α-actinin	filament cross-linking	100(x 2)	filopodia, lamellipodia, stress fibers
filamin (ABP-280)	filament connections at right angles	280	filopodia, stress fibers
spectrin	links to membranes	246 + 280	erythrocytes
ERM (ezrin, radixin, moesin) family proteins	filament cross-linking		cytoskeleton

Table 1. Some examples of actin binding proteins.

Actin stress fibers tend to form when the cell requires additional strength, such as in endothelial cells, in response to an elevated shear stress, or in migrating fibroblasts. These fibers often concentrate around and attach to focal adhesion sites, discussed elsewhere in the context of cell adhesion.

F-actin is also prominent in microvilli, the finger-like protrusions of the plasma membrane often found in cells involved in adsorption. These microvilli which increase the surface area of a cell can dramatically augment the rate of exchange between the cell and its environment. Both F-actin and G-actin are present at high concentration in filopodia (spike-like protrusions) and lamellipodia (broad, sheet-like extensions). In microvilli, actin may be present mainly to lend structural integrity, while in filopodia and lamellipodia, its role is thought to be

more dynamic and is critical to the process of initiating and extending these processes. Whereas this chapter focuses on the *structural* characteristics of the cytoskeleton, actin is also critical in many dynamic processes such as cell migration or muscle contraction, which are discussed later, in Chapter 2.3.

Intermediate filaments

The intermediate filaments (IF) of approximately 10 nm diameter appear to play primarily a structural role as they have not been identified to be involved in cell movement. Even their structural role, however, is not well delineated. The intermediate filaments are much less studied than actin and not as well characterized. Perhaps this is due to the fact that there is no single molecular constituent that comprises the intermediate filaments, instead, there are more than 50 different IF genes that have been identified. These can be classified into six groups based on similarities in their amino acid sequence.

Intermediate filaments constitute roughly 1% of total protein in most cells, but can account for up to 85% in cells such as epidermal keratinocytes and neurons (Fuchs and Cleveland, 1998). While they come in many varieties, they share a common structural organization. All have a central α-helical domain of over 300 amino acids with amino- and carboxy-terminal domains at the ends. As illustrated in Fig. 6, assembly occurs by the formation of dimers into a coiled coil structure. Then the dimers assemble in a staggered anti-parallel array to form tetramers that connect end-to-end to form apolar protofilaments. These protofilaments assemble into a rope-like structure containing approximately 8 each. (see also Fuchs and Cleveland for an alternative view). Although intermediate filaments are more stable than the microfilaments, they can be modified by phosphorylation. This occurs on a time scale typically longer than that for changes in the F-actin structures, however.

Intermediate filaments tend to be found near the nuclear envelope, extending outward, reaching to the plasma membrane (Fig. 3). As this arrangement suggests, intermediate filaments are thought to help anchor the nucleus in the cell. The structural role of intermediate filaments is reinforced by their presence, as keratin filaments, in epithelial cells, connecting to the plasma membrane at desmosomes and hemidesmosomes and helping to withstand mechanical stress. However , they exhibit a lower bending stiffness than either microfilaments or microtubules, as evidenced by their persistence length of only 1-3 μm.

Type	Protein	Size (kDa)	Site of expression
I	acidic keratins	40-60	epithelial cells
II	neutral or basic keratins	50-70	epithelial cells
III	vimentin	54	fibroblasts, WBC
	desmin	53	muscle cells
	glian fibrilary acidic protein	51	glial cells
	peripherin	57	peripheral neurons
IV	neurofilament proteins	60-150	neurons
	α-intermixin	66	neurons
V	nuclear lamins	60-75	nuclear lamina
VI	nestin	200	stem cells of CNS

Table 2. Various types of intermediate filaments

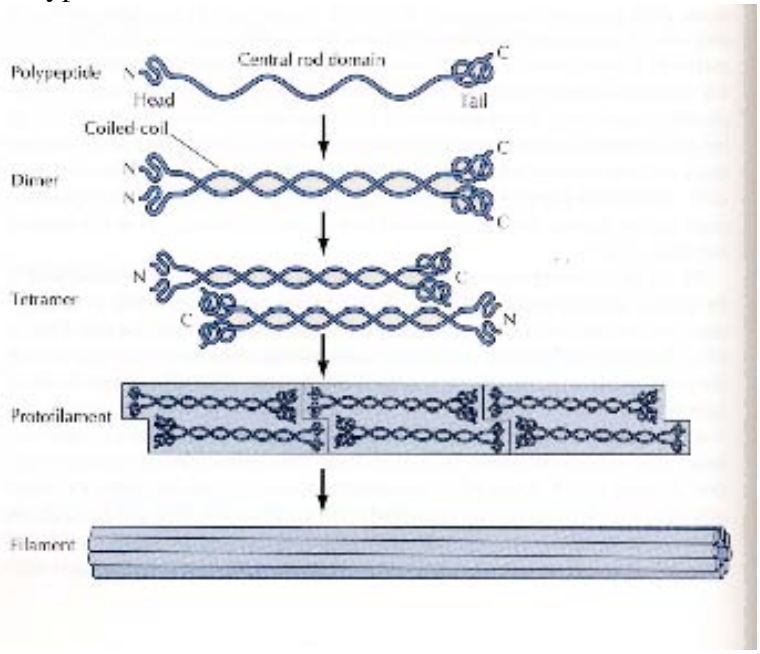

Fig. 6. Intermediate filament assembly

Linker proteins such as BPAG1 and plectin contain both actin and IF binding domains, providing a means by which these networks can be linked. Evidence also exists for plectin binding to microtubules.

It was mentioned earlier that the intermediate filaments are generally believed not to be important for cell growth or movement. This is based on experimental observations in which intermediate filament integrity has been disrupted with no observable effect on migratory or mitotic behavior.

Microtubules

Microtubules take the form of hollow rods with approximately 25 nm outer diameter and 14 nm inner diameter. By comparison to either microfilaments or intermediate filaments, microtubules are rigid structures, but exist in a dynamic equilibrium much as do microfilaments. To a large extent the microtubules determine cell shape and are important in cell mirgration, and especially during the process of mitosis (see Fig. 6-1). They also are central to the motion of cilia and flagella.

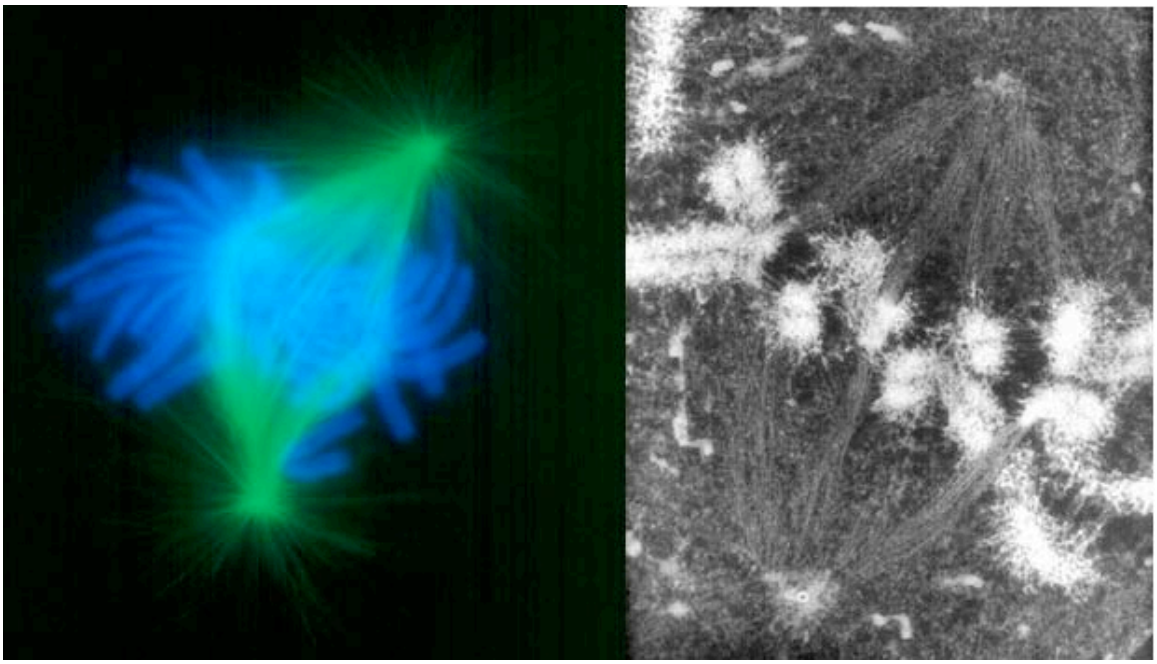

Fig. 6-1. A newt cell in the metaphase of mitosis. Left: Fluorescent image showing the microtubules, attached to the opposed spindle poles, in green and the chromosomes in blue. Right: Image of a similar cell obtained by high voltage electron microscopy. The microtubules provide the network along which the chromosomes move toward the poles. [Reproduced from http://www.wadsworth.org/BMS/SCBlinks/WEB_MIT2/res_mit.htm, C. Rieder.]

The tubular structures are comprised of tubulin, a globular dimer consisting of two 55 kDa polypeptides, α-tubulin and β-tubulin. The dimers polymerize to form microtubules that consist of 13 linear protofilaments forming a hollow-cored cylinder (Fig. 7). The filaments are polar having a rapidly growing end and a slowly growing end.

Both α-tubulin and β-tubulin bind GTP that regulates polymerization. The GTP bound to β-tubulin is hydrolized to GDP after polymerization. The GDP that remains bound to tubulin is less stable and can release from the ends of the microtubule. If the hydrolysis occurs too quickly, before new GTP-bound tubulin can bind to the end, the microtubule might disassemble.

This can lead to what is termed "dynamic instability" in that, depending on the rate of hydrolysis and rate of GDP-bound tubulin addition to the end, the microtubule can either grow or shrink (Mitcheson, Kirschner, see also Ch. 3.4). In fact, free ends tend to alternate between periods of steady growth and disassembly in a stochastic manner.

Measurements have indicated that because of this dynamic process, the half-life of a microtubule is typically only several minutes. This time can vary considerably, though, and is likely much shorter during mitosis, during which the microtubules play a critical role and need to undergo even more rapid turnover. The importance of microtubule assembly during mitosis has been demonstrated by the effect that tubulin binding agents such as colchicine and colcemid have on cell division. This prevents the addition of monomers to the microtubule and, as a consequence, prevents mitosis entirely. Because of this capability, related drugs such as cristine and vinblastine are used as chemotherapy for cancer. Another cancer drug, taxol, stabilizes microtubules and thereby also blocks mitosis.

During interphase, microtubules tend to be anchored (at their negative ends) to the centrosome, located near the nucleus. From there they extend to all parts of the cell, suggesting a strong role in maintaining the structural integrity of the cell. Microtubules also play a role in intracelllular transport of vesicles and organelles, beating of cilia and flagella when in conjunction with motor proteins such as the kinesins and dyneins (discussed in Chapter 2.3). In many of these situations, the microtubule is thought to play a structural role that relies on it having a high bending stiffness. Measurements (Gittes et al., 1993) have, in fact, determined the bending stiffness ($K_b = E_f I$) of isolated microtubules based on their thermal fluctuations and found it to be on the order of 2.6×10^{-23} N·m^2. This may not seem very large, but given its diameter, and that the moment of inertia varies as the fourth power of radius, this is really quite an impressive value.

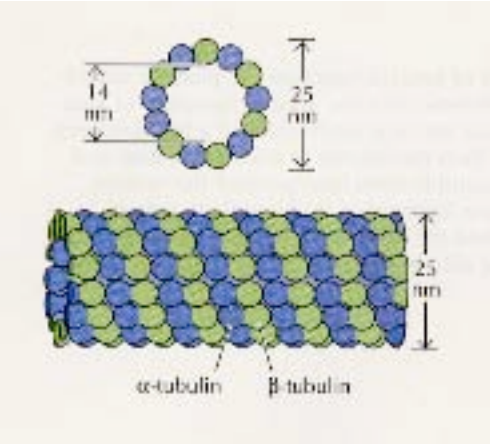

Fig. 7. Schematic of microtubule assembly.

	Diameter, $2a$ (nm)	Persistence length, l_p (μm)	Bending stiffness, K_B (Nm^2)	Young's modulus, E (Pa)
Actin filament	7	15	$7x10^{-26}$	$\sim 2x10^9$
Microtubule	25	6000	$3x10^{-23}$	$\sim 2x10^9$
Intermediate filament	10	1	10^{-26}	$\sim 4x10^6$

Table 3. The main constituents of the cytoskeleton, and their mechanical properties. Note that the Young's modulus, estimated using the diameter and bending stiffness values for actin filaments and microtubules, is approximately the value that would be predicted on the basis of van der Waals attraction between two surfaces (J. Howard, 2001). Recall that the persistence length and bending stiffness are related through the expression $l_p = K_b / k_B T$, and that $K_b = EI = E\frac{\pi}{4}a^4$ for a rod of circular cross-section.

2.2.3 Mechanical properties of the cytoskeletal network

As is evident from the discussion of the last section, the cytoskeleton consists of a complex biopolymer network with varying degrees of interconnection, existing in a state of dynamic equilibrium. The dynamic state arises from the continual polymerization and depolymerization of the constituent filaments and the changing density of cross-links between filaments of the same or different family. This picture is complicated further by the milieu of other intracellular constituents that may or may not affect structural properties exhibited by the cell.

To make progress in understanding the mechanics of the cytoskeleton, we will focus on those filamentous components discussed earlier, the F-actin, intermediate filaments, and microtubules. We will also simplify by making plausible conjectures about the geometry of the structure and its state within the cell in the absence of external forces.

Our objective in this section is to come to a better appreciation of how the elastic properties and geometric arrangement of the constituent filaments give rise to the elastic properties observed by the various experimental methods just described. These experiments have shown that the elastic modulus of cells can vary considerably from one cell type to another. Cells of the epidermis, for example, require greater structural integrity than the red blood cells subjected to the relatively low shear stresses in the blood. Even within a given cell type, the elastic properties can change. Skeletal muscle, for example, changes its modulus by over an

order of magnitude within a small fraction of a second. Other cells change too, but more often over a longer time period, in response, for example, to changes in their mechanical environment.

To help put these measurements of stiffness in context, consider the data presented in Fig 8. According to the various measurements that have been made, cells seem to range in shear modulus from about 10 to 10^4 Pa (see Table 4), and therefore exhibit a stiffness somewhat lower than collagen gels at low concentration (or common gelatins) or relaxed skeletal muscle. (Allow your leg to relax completely, then feel the stiffness of your calf to get a sense for an elasticity of about 10^4 Pa.) This range probably says more about differences in the models used as a basis to infer the shear modulus from the data than it does about real cell-to-cell variations. At best, these numbers inferred from experiment should be viewed as measures of an "effective stiffness" and comparisons between different measurement methods and interpretation should be made with caution. Nonetheless, since cells vary widely in their function, it would be surprising if their mechanical properties were not also variable. Other biological materials (e.g., bone, wood) exhibit a much higher modulus, but not because of their cellular content. Rather, their high stiffness is due to the calcification in bone and the collagen matrix found in wood and most plants. In tissues, too, the stiffness we measure is more often associated with the extracellular matrix with its elastin and collagen, than the constituent cells.

The elastic moduli of the cytoskeletal filaments are also shown in the figure. Notice that the filaments themselves (F-actin, intermediate filaments, and microtubules) all exhibit moduli much greater than the measured modulus of the cytoskeleton. These two must be

Fig. 8. The Young's modulus for a range of materials.

related in some way, but the connection is not immediately obvious. In Section 2.2.4 we explore different approaches that have been developed to relate the properties of the individual fibers to those of the assembled network. First, though, we discuss some of the methods that have been used to describe cell elasticity. Some of these methods are developed more fully in Chapter 1.2. Here we provide a brief review in the context of problems in cytoskeletal mechanics.

2.2.4 Experimental measurements of cell elasticity

Essentially any intervention that produces deformation of the cell can, and often has, been used to infer its mechanical properties. Many of these methods derive from common engineering usage while others have been developed specifically for the purpose of examining the mechanical properties of a cell. Taken as a group, these methods form the basis for all current knowledge of cell mechanical properties and it is therefore appropriate that we focus our attention on the methods that have been used and continue to be developed. In interpreting these data, however, note that whenever the cell is deformed, its response reflects not only the elasticity of the cytoskeleton, but also of the lipid bilayer, and depending on the rate of deformation, perhaps the viscosity of cell constituents as well. Its deformation will depend on the cell dimensions and its external tethering. Furthermore, the cell is neither homogeneous, consisting of organelles, ribosomes, and numerous other structures, making it difficult to interrogate one isolated constituent, nor isotropic. In much of what follows, we treat the membrane and cytoskeleton as ideal, isotropic, homogeneous materials, either purely elastic or viscoelastic, while recognizing the simplifications this implies. Later in this chapter, we take a closer look at the microstructure of the material to see how these measured properties relate to the characteristics and deformations of the fibrous constituents of the matrix. Finally, it is important to recognize that these experimental results, while useful in their original, unprocessed form, normally are interpreted in the context of a particular model. In many of the models, for example, the effect of the cell membrane is completely neglected, and the cell is treated as an elastic or viscoelastic continuum. Consequently, reported values for such properties as the Young's modulus or shear modulus depend not solely on the measurement, but also on the particular model used in the process of data analysis.

Cell poking and squashing (indentation analysis)

This test is one of the simplest methods to probe for cell stiffness, but as with all methods, the results obtained need to be carefully interpreted. In principle, one need only push against the cell with a known force and measure the displacement of the probe; for a given force, a stiffer cell

will allow a smaller deflection than a compliant one. To interpret this measurement, the cell is taken to be large compared to the size of the indenter (of radius a), as well as compared to the deflection of the probe into the cell (δ), in order that the cell can be viewed as an elastic half-space (Fig. 16). It will also be useful to assume that the cell can be treated as an elastic continuum in that the microstructure has a characteristic length scale small compared with either a or δ (Fig. 16b). If so, we can treat the cell as having a homogenous composition, neglecting the fine-scale structure of the constituent filaments. It is further assumed that the cell membrane contributes little to the stiffness of the cell, and that the cell behaves as a linearly elastic material with Young's modulus E and shear modulus G. While neglect of the cell membrane clearly contradicts some of the findings just discussed in Chapter 2.2, it appears to be a reasonable approximation for some cell types and, in any event, provides the opportunity to focus attention on the cytoskeleton. We will also consider the cytoskeleton to be incompressible for now. Under these assumptions, a simple scaling analysis provides some instructive guidance.

For the situation shown in the figure, in which a cell is indented by a probe with a blunt surface, the volume of the region within which the cell matrix is significantly deformed scales as a^3. Within this region, the deformations are of order δ, so that the localized strains (ε) are of order δ/a. The strain energy density scales as $\tau\varepsilon \sim E\varepsilon^2$, so the total strain energy $\sim E\varepsilon^2 a^3$. The work done by the indenter in producing this deformation is $F\delta$. Equating these, we obtain:

$$F\delta \sim E\,(\delta/a)^2 a^3 \tag{56}$$

or

$$E \sim G \sim F/(\delta a) \tag{57}$$

This suggests a linear relationship between the applied force and the displacement of the probe, consistent with measurements made in lymphocytes (Fig. 17).

The scaling analysis that led to eqn. (57) is not capable of providing the dimensionless coefficient necessary to produce an equality. That is, it fails to determine the constant c in the expression:

$$F = cG\delta a \tag{58}$$

or

$$G = F/(c\delta a) \tag{59}$$

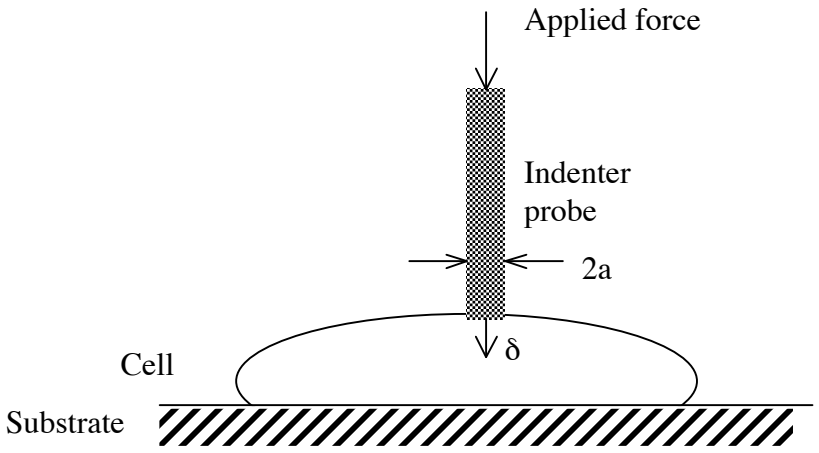

Fig. 16. Cell poking experiment.

To determine the numerical value of c in Eqn. (59) requires either an experiment with a material of known shear modulus or a more rigorous analysis. The analysis, performed based on the assumptions stated previously, is a solution of the governing equations (7)-(9), representing an internal force balance and the constitutive relation that describes the nature of the material for an isotropic, Hookean elastic solid. Solution of these equations (see e.g., Johnson, 1985), with boundary conditions describing a uniform displacement over the region of contact between the (blunt) indenter and the cell surface gives rise to a solution of the same form of equation (59), but with the constant c given as 8.

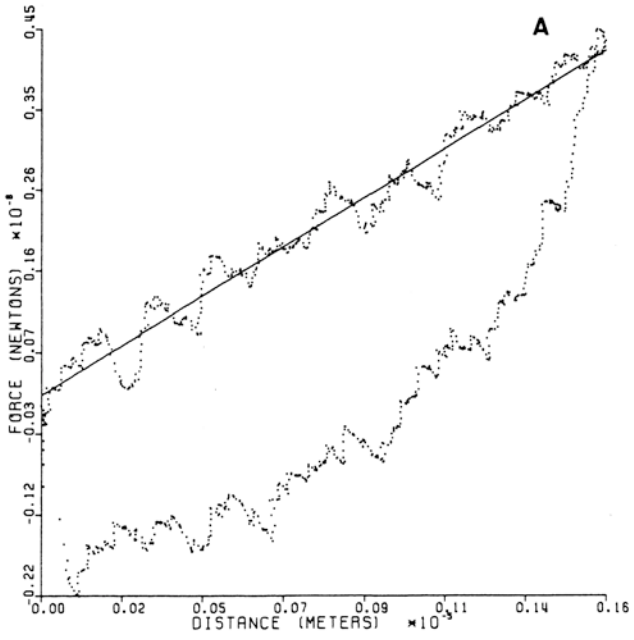

Fig. 17. Experimental measurements made by cell

Using this method in conjunction with the experimental data of Fig. 17 for example gives an estimate for the shear modulus of the lymphocyte of about 300 Pa and for a neutrophil about 100 Pa. Both of these increase when the cell is activated (Zahalak et al., 1990). Once we have the value of the shear or Young's modulus, along with an estimate for the Poisson ratio, we can predict the response of the cell to other types of loading, using the methods described in Ch.1.2 for an elastic continuum.

Interpretation of the experimental results is, however, not quite as straightforward as this analysis might suggest. One complication that can immediately be seen is that the cell response is not purely elastic; if it were, the two curves in Fig. 9 corresponding to the forward and reverse movement of the probe would be superimposable and not exhibit the hysteresis seen in the figure. The fact that they are not indicates that the cell is not purely elastic, but rather, that it behaves in a viscoelastic manner. It can therefore be analyzed using the approach presented below for a viscoelastic continuum. In this instance, it is convenient to begin with the integral formulation, eqns. (5) - (6). The expression relating force to deformation for an elastic solid (eqn. (58)) can be seen to be similar in form to eqn. (6) where *k(t)* takes the role of *8Ga* with *G* being the shear modulus, and the integral expression (eqn. (6)) can be re-written in the following form using the *elastic-viscoelastic correspondence principle* (Christensen, 1971)

$$F(t) = 8a\int_0^t G(t-\tilde{t})\left(\frac{d\delta(t-\tilde{t})}{d\tilde{t}}\right)d\tilde{t} \tag{60}$$

where the integration begins at time t=0 when the probe begins its descent. If the cell were comprised of a viscous liquid, $G(t) = \mu\delta_k(t)$, where μ is the Newtonian viscosity of the liquid and $\delta_k(t)$ is the Kronecker delta. Noting that in the present experiment, $d\delta / dt = v = const$, the viscous contribution to the force can be written:

$$F_v = 8a\int_0^t \mu\delta_k\left(t-\tilde{t}\right)\frac{d\delta\left(\tilde{t}\right)}{d\tilde{t}}d\tilde{t} = 8av\mu \tag{62}$$

Thus, to a reasonable approximation, the viscoelastic cell can be thought of resisting the motion of the probe through a combination of the elastic and viscous contributions to force, or:

$$F\left(t\right) = 8a\left[G\delta + \mu v\right] \tag{63}$$

Comparing this to eqn. (58) and noting that $\delta = vt$ in this experiment, we see the strong similarity between the two expressions, and the significance of the effective viscosity term which decreases in importance as the rate of deformation is slowed. At rates rapid enough for viscoelastic effects to be seen, the presence of viscoelasticity exhibits itself by an upward movement of the force-displacement curve while the probe is moving into the cell, as can be seen in some of the Zahalak [4] experiments. When the probe is reversed, the effects of viscosity are clearly evident

as indicated by the hysteresis of the curves and, though not considered here, can be analyzed by the same procedures.

Micropipette aspiration

Micropipette aspiration is an alternative to the indentation test in which the cell is drawn into a small-bore pipette (Fig. 18). In this case, the result is an experimental relationship between the aspiration pressure Δp (below the reference pressure around the cell) and the distance δ into the pipette that the cell is drawn. The pipettes that are used are typically on the scale of a few microns in diameter, similar to the imposed deflections. These dimensions roughly satisfy the constraints mentioned in the context of indetation studies, that $l << a \sim \delta << L$ where l is the characteristic length of the microstructure and L is the cell dimension, suggesting that a continuum analysis would be a reasonable approach.

The scaling analysis proceeds in a manner similar to that used for the indenter and the cell is assumed to be composed of a Hookean elastic solid that can be treated as a continuum. In this case, however, two lengths characterize the pipette: the inner and outer radii, a and b, respectively. The result obtained is analogous to the one given above for the indenter, except that the applied force F in the previous case is now replaced by the force

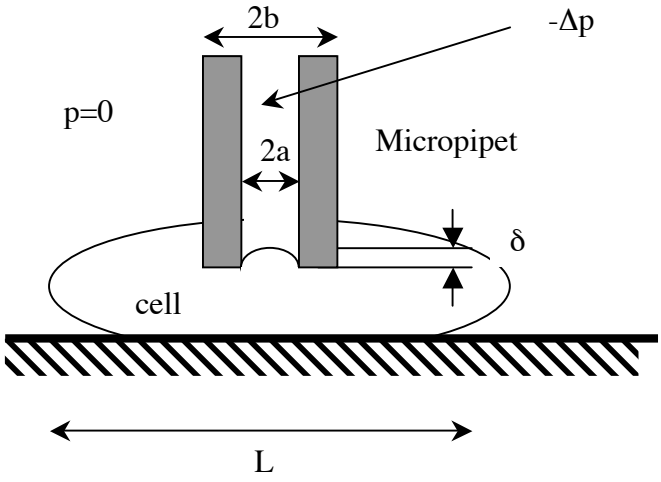

Fig. 18. Schematic of a micropipette aspiration experiment.

due to pressure, $\Delta p \cdot a^2$. The result is the scaling prediction

$$E \sim \Delta p \, (a/\delta) \tag{64}$$

where we have assumed that the important length scale for the deformations inside the cell is a rather than b. Alternatively, we can consider the limit as b approaches a, in which case the two characteristic lengths collapse into one.

Also similar to the indenter, a more rigorous analysis can be performed to obtain the constant of proportionality in the above relation, which in this case gives

$$E = \frac{3}{2\pi}\frac{a}{\delta}\Delta p \cdot \Phi\left(\frac{b}{a}\right) \tag{65}$$

where for b/a in the range of 1.1 to 2.0, $\Phi(b/a)$ lies between 2.2 and 1.4.

Experimental results are typically plotted in terms of the distance of deformation into the pipette as a function of the pressure reduction in the micropipette. The result is seen to be quite linear for an endothelial cell (Fig. 19) consistent with the form of eqn. (9), which, by comparison to analytic predictions (see Theret [10]), gives values for the Young's modulus in the range of 200 to 800 Pa. Interestingly, exposure of these cells to shear stress of 3 Pa increases E consistent with the observation of new stress fibers organizing in the cytoskeleton

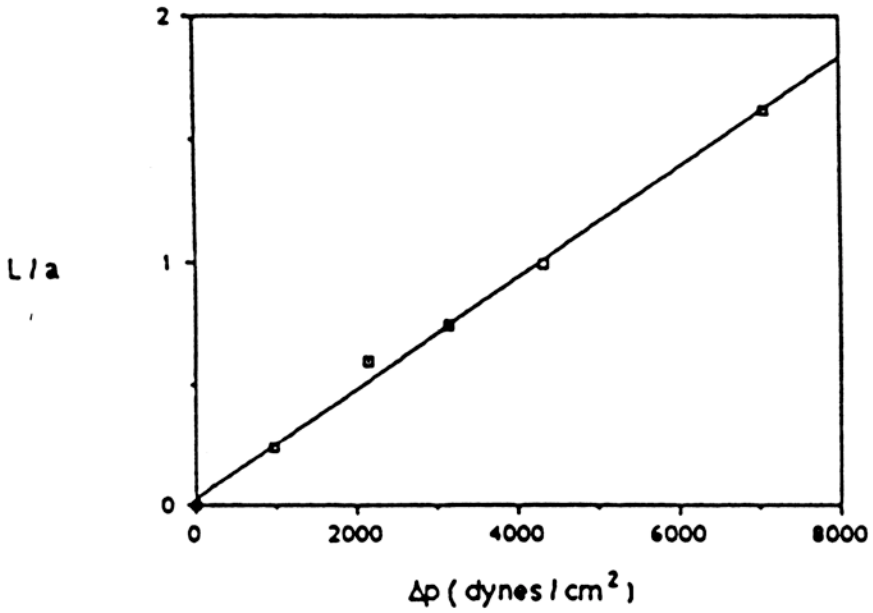

Fig.19. Experimental result obtained on a from an endothelial cell micropipette experiment (reproduced from Theret et al., 1988).

It is important to reiterate that in both of these cases, indentation and micropipette aspiration, we have neglected the stiffness of the membrane. Incorporating its effect would tend to reduce these estimates of cytoskeletal elastic modulus. In the case of the lymphocyte, micropipette experiments (Evans & Yeung, 1989) have suggested that the membrane behaves as

though it were under a constant surface tension, independent of the amount of surface strain, of $3.3x10^{-5}$ N/m.

Magnetic twisting cytometry

The indentation and micropipette aspiration methods provide a measure of the elasticity of a single cell. By contrast, magnetic twisting cytometry (MCT) interrogates many cells simultaneously, giving a single output representing an average over many cells. This has some advantages in that it eliminates the need to do many individual measurements of obtain a result characteristic of a cell population, but also has some drawbacks in terms of being less amenable to direct interpretation.

In this technique, ferromagnetic microspheres are coated with a ligand (e.g., a synthetic peptide containing the RGD sequence) having an affinity for a particular cell receptor (e.g., the integrin receptors). Binding to integrins assures strong linkage with the cytoskeleton, although other, non-cytoskeletal receptors can also be used to probe the differences in stiffness as a function of cytoskeletal tethering. These ligand-coated beads are then added to a population of cultured cells and allowed to bind. Once binding has occurred, the beads are magnetized by application of strong magnetic field with a specific orientation. Then, a second magnetic field is imposed, perpendicular to the first, applying a twisting torque to the beads and causing them to rotate. This rotation is monitored by a magnetometer that measures the strength of the remnant field in the direction of the original magnetization. Individual bead displacement can also been observed to avoid artifacts associated with averaging over large numbers of beads with varying degrees of attachment. After some degree of rotation has occurred, the twisting field is turned off and the cells are allowed to relax. This sequence is illustrated in Figs. 20 and 21 with the corresponding mean rotations. The magnetic field can also be subjected to harmonic variations in torque over a range of frequencies to measure the storage and loss moduli of the cell.

With the MTC method, the beads are subjected to a torque so the resulting deformation of the cell is quite complex compared to that for either of the two cases considered thus far. As the bead rotates (Fig. 20) the membrane and cytoskeleton are both deformed. Perhaps more importantly, for a bead twisted in the clockwise direction, the right hand surface of bead might come in direct or near contact with the cell and the possibility exists that the number of binding sites will increase during the period of twist. Similarly, stress on the binding sites on the left-hand surface of the bead will be high, possibly high enough to cause some of these bonds to be disrupted. Either or these effects would both tend to prevent the bead from returning to its initial orientation and may explain some of the non-reversible rotation seen in the experimental data (Fig. 21).

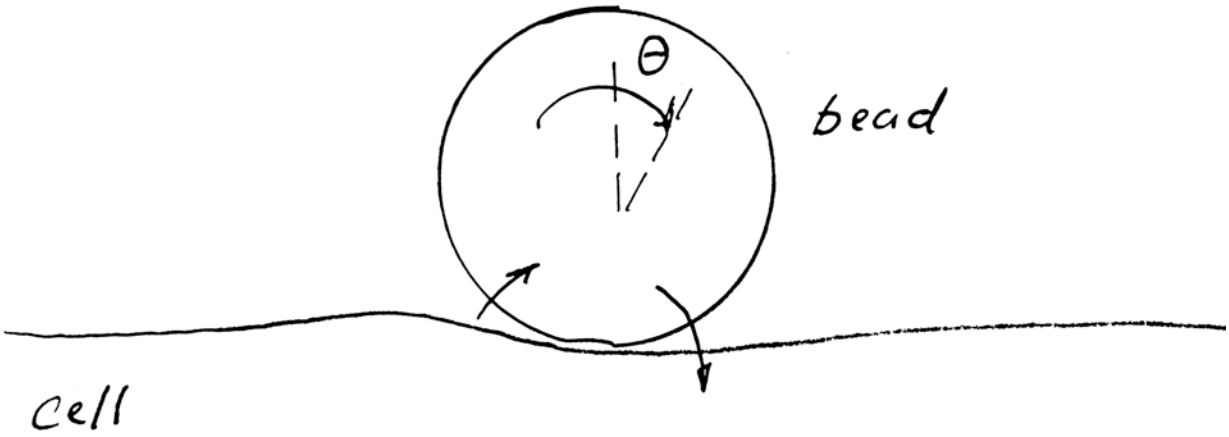

Fig. 20. A schematic showing the forces and deformations produced by magnetic twisting cytometry.

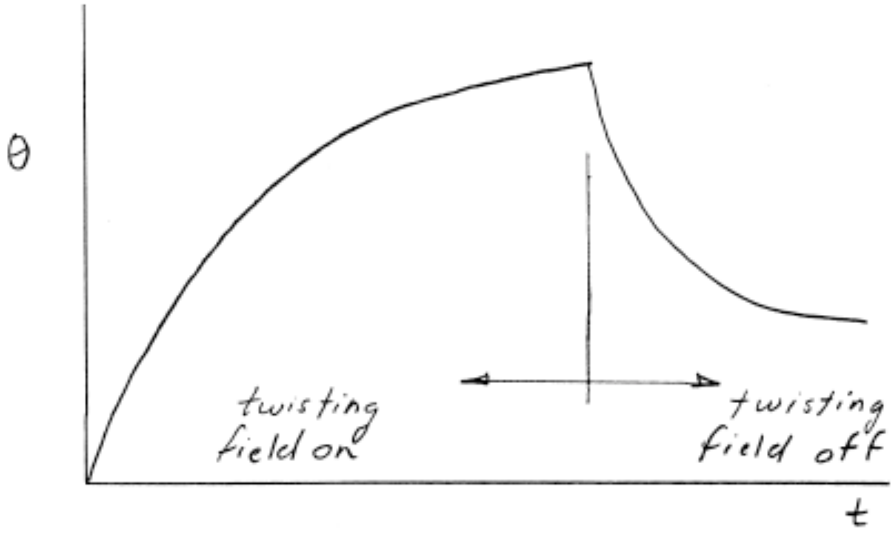

Fig. 21. Typical experimental results obtained by magnetic twisting cytometry. The twisting angle θ can be viewed either as the rotation of a single bead, or the average rotation of a large population of beads, depending on the experiment.

The interaction forces between the bead and the cell membrane are sketched in qualitative terms in Fig. 20, and consist of both shear and normal stresses, tensile and compressive. If the region of contact between the bead and cell membrane is characterized by the contact radius a, and the rotation of the bead is small, then a balance of moments leads to the following scaling relation:

$$\Theta \sim a^3 \tau \tag{66}$$

where Θ is the torque applied to the bead by the magnetic field, since the force of interaction scales with the product of the peak stress and the area of contact, and the moment arm scales with a. The work done by the rotation is $\Theta\alpha$ where α is the (small) angle of rotation. Stresses (primarily shear) induced in the cell lead to strain energies that scale as $\tau\varepsilon a^3$ where $\varepsilon \sim a\cdot\alpha/a \sim \alpha$ and $\tau \sim \varepsilon G$. Equating these, one obtains

$$G \sim \Theta/(\alpha a^3) \tag{67}$$

One of the advantages of this method is that by careful selection of the ligand used to coat the bead, it is possible to selectively bind to specific families of cell surface receptors that differ in terms of the nature of their attachment to the cytoskeleton. This therefore allows the possibility to probe more selectively than in the indenter or micropipet methods.

When oscillatory torques are applied and bead displacement rather than rotation is measured, the data are analyzed differently. A ratio is formed between the complex torque T^* and the resulting complex displacement δ^*, defining a new measure of elastic stiffness g^* with units of Pa/nm. A relationship between g^* and G^* is obtained by finite element analysis of a bead being rotated on a homogeneous, elastic material of given dimensions approximating those of a cell. Taking a representative value for this parameter, and assuming it to be independent of frequency, the results of Fig. 22 are obtained for the storage and loss moduli. Notably, the data obtained in this manner for different cells and with a variety of biological manipulations all conformed to the following empirical expression (solid lines in Fig. 22):

$$G^* = G_0\left(\frac{\omega}{\omega_0}\right)^{x-1}(1+i\bar{\eta})\Gamma(2-x)\cos\left[\frac{\pi}{2}(x-1)\right] + i\omega\mu \tag{68}$$

where G_0 and ω_0 are scale factors, $\bar{\eta} = \tan(x-1)\pi/2$, Γ denotes the gamma function, μ is a

Newtonian viscosity, and x is a parameter that characterizes the transition between solid-like (x=1) and fluid-like (x=2) behavior. The data fits seen in the figure were obtained using a single value each for G_0 and ω_0, leaving only x and , to a lesser extent, μ, to vary for different sets of

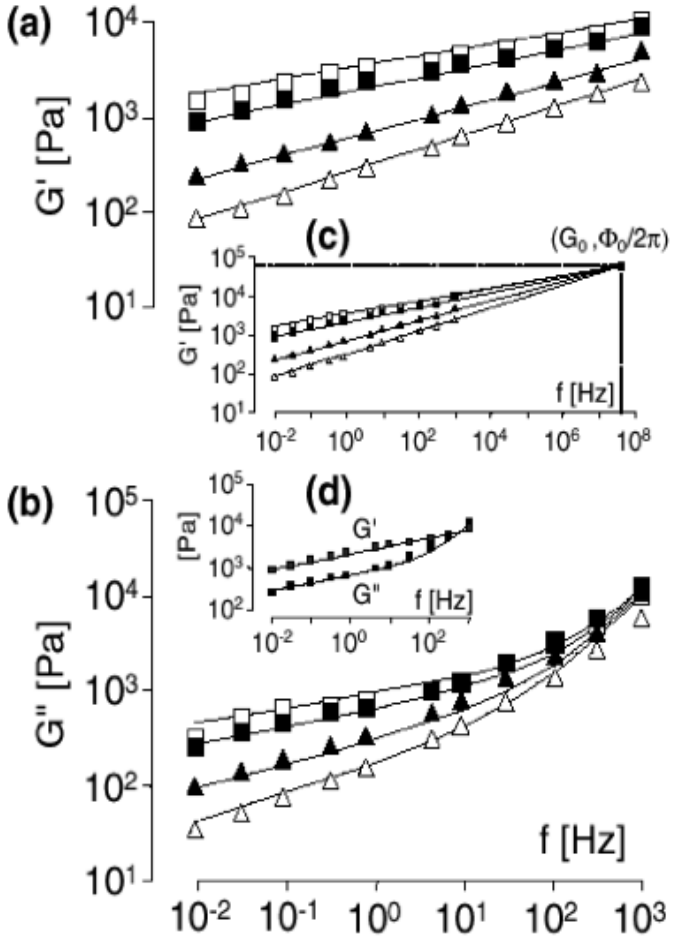

Fig. 22. Storage (a) and loss (b) moduli plotted over 5 decades of frequency for smooth muscle cells under control conditions (solid squares), after treatment for 10 minutes with histamine to produce smooth muscle activation (open squares), an agent to eliminate baseline tone, DBcAMP (solid triangles), or cytochalasin D, to disrupt actin filaments (open triangles). (c) shows the extrapolation of the data for G' illustrating the intersection at high frequency, and (d) directly compares the data from (a) and (b) under control conditions. Solid lines are the fit to the data by eqn. (68) with G_0=53.6 kPa and ω_o =2.510^8 rad/s . (Reproduced from Fabry, et al., 2001)

data. Similarity of these results with predictions for a soft glassy material suggest the possibility of a common physical basis that is still being explored.

Laser and magnetic tweezers

Beads that are either attached to the cell surface via receptor ligand bonds, or internalized by the cell through phagocytosis, can be forced either by the use of a magnetic or optical trap or tweezers. A magnetic trap acts in much the same manner as the MTC just described, on either paramagnetic or ferromagnetic beads, the difference being that a force, rather than a torque, acts on each particle. The force can be either constant, or oscillatory with the latter being useful for the purpose of obtaining estimates for the frequency dependence of the elastic moduli. In the case of an optical trap, the particle merely has to have a different index of refraction than the

surrounding medium, and the force, provided by a focused laser beam, relies on the deflection of the beam and the corresponding change in photon momentum (see Chap. xx for a complete description).

Each method has certain advantages and disadvantages. With a magnetic trap, force is controlled by the strength of the applied magnetic field and varies as the square of the field strength as seen from the following expression for paramagnetic beads:

$$F(t) = \mu_0 \chi V \nabla(\vec{H} \cdot \vec{H}) \tag{69}$$

where χ is the volume susceptibility, μ_0 is the permeability constant, V is the bead volume and $\vec{H}$ is the local, time-varying field strength. Thus, if the local field strength is known as well as the magnetic characteristics of the particle, the force can be accurately controlled. Forces on the order of 10 nN have been produced using single-pole magnets brought to within 10-100 μm of the bead. While single pole traps offer the potential for greater forces, they have the disadvantage, however, that the field strength is spatially non-uniform. In order to produce more uniform fields, multiple-pole traps have been designed, but these are typically only capable of generating forces on the order of 100 pN. Displacement, in this case, depends on the applied force and the elastic or viscoelastic properties of the cell, and is determined by direct observation of the bead motion.

In the case of the optical trap, moving the focal point of the laser controls the position of the bead. Force measurement, however, is more difficult since it relies on a precise calibration of the force well in the vicinity of the laser focal point and the ability to measure small displacements of the bead from the point of equilibrium. A further disadvantage is that forces only up to about 10 pN can be generated on a micron size particle by an optical trap with ~1 W of laser power, below the damage threshold for living cells.

Data analysis depends on whether the bead is attached to membrane receptors or internalized by the cell. For beads inside the cell, and assuming the cell can be treated as a homogeneous, incompressible viscoelastic continuum extending to infinity, acted on by a time varying force *F(t),* the equation of motion is given by

$$F(t) = 6\pi a\left(G'x + \mu \frac{dx}{dt} \right) \tag{70}$$

(for the elastic solution, see Lin et al., Summer Bioengineering Conferrence, 2003) where x is the bead displacement in the direction of forcing, G' is the storage modulus and μ the viscosity of the medium. The second term can be seen to be the expression for Stokes drag on a sphere

whereas the first is the elastic contribution, representing the force required to move a sphere a distance x in an infinite elastic medium with shear modulus G'. In the case of oscillatory forcing, Eqn. (70) can be written using complex notation, substituting $F(t) = F_0 \exp(i\omega t)$ and $x(t) = x_0 \exp[i(\omega t + \phi)]$, leading to the following expressions for the storage and loss moduli (Zeimann, Radler and Sackmann, 1994):

$$G' = \frac{F_0 \cos\varphi}{6\pi a x_0} \tag{71}$$

and

$$G'' = \frac{F_0 \sin\varphi}{6\pi a x_0} \tag{72}$$

noting that the quantity $\mu\omega$ is equivalent to the loss modulus, G''.

If the bead is tethered to the membrane, then the analysis and forcing is tangent to the plane of the membrane, then the situation is somewhat more complicated. The simplest approach would be to say that the membrane can still be neglected, and to a first approximation, that the cell surface remains planar under forcing, leading to the estimate that the displacements for a given force are twice what they would be for the bead totally immersed in a viscoelastic medium. In that case the above analysis could still apply, except that the numerical factors in eqns. (71) & (72) would change from 6 to 3. Alternatively, the membrane can be taken into account explicitly which naturally leads to a considerably more complicated result (see e.g., Boulbitch, 1999).

AFM methods

A variation on the cell indentation technique involves the use of an AFM probe to apply the time-varying force. The advantages of this approach are that the force can be oscillated over a range of frequencies facilitating the calculation of the complex shear modulus G^*, and that the probe can be scanned over the cell while oscillating, thereby producing an elasticity map of the cell surface.

In one application of AFM to obtain $G^*(\omega)$ at a fixed point in the cell, a small spherical bead was attached to the AFM tip so that the Hertz contact model could be used for data

interpretation. In this model, an elastic half-space is indented by means of a sphere of radius a, giving the following relationship between the applied normal force F and the indentation δ. [2]

$$F = \frac{4}{3}\sqrt{a\delta^3}\,\frac{E}{1-\nu^2} \tag{73}$$

This expression was extended for small oscillations of magnitude $\tilde{\delta}$ superimposed on a mean indentation δ_0 for a viscoelastic material (Mahaffy, Shih, MacKintosh, and Kas) to yield:

$$F \approx \frac{4}{3}\sqrt{a\delta^3}\,\frac{E}{1-\nu^2} + \frac{3}{2}\bar{E}^*\tilde{\delta}\sqrt{\delta_0} \tag{74}$$

where $\bar{E}^*$ is defined as the frequency-dependent part of $E/(1-\nu^2) = 2\left[(1+\nu)/(1-\nu^2)\right]G^*$ and $\bar{E}_0$ is the zero frequency limit of $2G'(1+\nu)/(1-\nu^2)$. Considering only the oscillatory component of this force F_{osc}, the following expression for the complex shear modulus can be obtained:

$$G^* = G' + iG'' = \frac{1}{4}\left(\frac{1-\nu^2}{1+\nu}\right)\frac{F_{osc}}{\tilde{\delta}\sqrt{\delta_0 a}} \tag{75}$$

for situations in which $|\tilde{\delta}|/\delta_0 << 1$ where F_{osc} and $\tilde{\delta}$ are both complex quantities.

In experiments conducted on NIH3T3 fibroblasts, static values for $E/(1-\nu^2)$ ranged between 1-2 kPa. When the bead was oscillated at frequencies between 50 and 300 Hz with oscillation amplitudes of 5-20 nm, values for the real and imaginary parts of $|\bar{E}^*|$ both fell in the range of 1-10 kPa with the loss modulus contribution increasing significantly over this frequency range.

AFM can also be used in a different way that makes effective use of its ability to probe larger surfaces. As the probe traverses a specimen such as a cell, it can be sequentially used to indent the cell at each location, simultaneously measuring the applied force and the displacement. In this sense, it acts in the same manner as cell indentation described above, except that it can repeat this procedure many times on a single cell, using a probe with tip dimensions on the scale of several nanometers, producing a stiffness map of the cell (Fig. 23(A)). Data are analyzed using a form of the Hertz contact model, modified for a pointed, conical tip, and corrected for the force required to deflect the AFM cantilever arm. If it is further assumed

[2] Note that this expression differs from the scaling suggested by eqn. (56). This is due to the assumption, in this instance, of a spherical tip in which case the area of contact between the probe and the cell membrane increases as the applied force is increased.)

that the material deformations are quasi-steady so that viscous contributions can be neglected, the shear modulus can be calculated from (Haga, et al., 2000):

$$G = \frac{\pi}{4\delta^2}\frac{F(1-\nu)}{\tan\alpha} \tag{76}$$

where α is the half-angle of the conical tip. When interpreted in this manner, the assumption being made, as mentioned before, is that the material is a homogeneous elastic continuum, thus neglecting the effect of the membrane and the discrete filament structure of the cytoskeleton. Interestingly, the stiffness map in Fig. 23 clearly delineate the actin

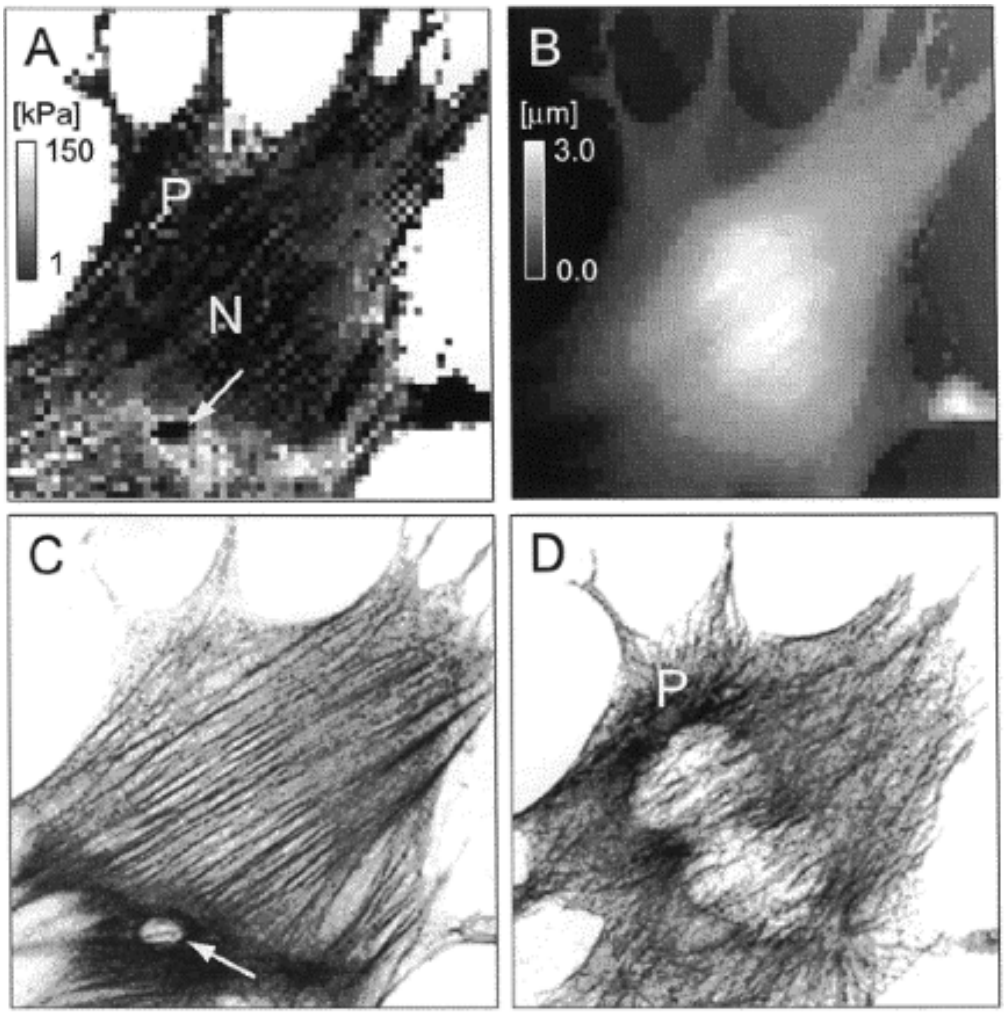

Fig. 23. Elasticity mapping in a fibroblast (NIH3T3) cell using atomic force microscopy. The elasticity map (A) shows gross differences with the lowest values corresponding to the nucleus (N), and a small pocket (arrow) low in actin content. The height of the cell from the substrate is

shown in (B). The two lower images are strained for actin (C) and microtubules (D) from the same cell. (Reproduced from Haga, et al., 2000)

filament matrix (though not the network of microtubules), suggesting that at least the second of these assumptions is violated. Nonetheless, this method provides the only means currently available to obtain such detailed information on the relative stiffness of different cell components, in this case showing that the nucleus is more compliant than the rest of the cell, with values for the Young's modulus (assuming ν=0.5) ranging from ~4 to 100 kPa.

Laser tracking microrheology (Yamada, Wirtz and Kuo, 2000)

One of the inherent drawbacks of all the methods described so far, is that they each involve the external application of force to a cell via a foreign body. This inevitably elicits a biological response from the cell, either through receptor bonding or by the application of force, that could alter the structural characteristics being measured. Indeed, micrographs of the cytoskeleton in the vicinity of adherent beads showed marked changes just minutes after bead attachment (Maksym et al., 2000). Any method, therefore, that minimizes such disruptions to the cell, leaving it in its normal, quiescent state, would have significant advantage.

Laser tracking microrheology (LTM) measures the viscoelastic properties of the cell by monitoring the Brownian motion of spherical particles embedded in the cell. While the particles might be small microspheres that are introduced by phaogocytosis, alternatively, the method can also be applied to spherical granulocytes that are naturally found in many cell types. In the latter case, disruption to the cell is kept to a minimum giving this method clear advantages over others.

Particle motion in LTM is detected by deflections in the forward scattered light from a single particle located at the focal point of a low-power laser. Following calibration, this allows the measurement of the mean squared displacement (MSD) of a particle's path relative a fixed reference point, computed as

$$MSD = \left\langle \Delta R^2(\tau) \right\rangle = (1/n)\sum_n \left[\left(\vec{r}(t+\tau) - \vec{r}(t) \right)^2 \right],$$

where τ is the elapsed time between the two measurements (obtained from a two-dimensional image). The *MSD* is measured over a large range of time scales to distinguish between viscous materials for which $MSD \propto t$ and elastic ones for which $MSD \sim constant$. In the more general case of a viscoelastic material, the complex shear modulus can be obtained from the following approximation for the unilateral Laplace transform of the shear modulus (Mason & Weitz, 1995):

$$\tilde{G}(s) = \frac{2k_B T}{3\pi a s \left\langle \Delta \tilde{R}^2(\tilde{s}) \right\rangle} \tag{77}$$

where *s* is the complex Laplace frequency, appropriate for the two-dimensional *MSD*. Implicit in this expression are the assumptions that Stokes law for the force on a sphere traveling at speed *V* *($F=6\pi a\mu\delta$)* can be generalized to a viscoelastic material, that the material can be treated as a homogeneous continuum, and that the particle is a rigid sphere.

It is useful to examine this expression in the two limits of a viscous liquid and an elastic solid. In the case of a viscous liquid, the *MSD* in two-dimensions would vary as $4D_0t$, where D_0 is the diffusion coefficient of the particle, given by the Stokes-Einstein relation to be $k_BT/6\pi\mu a$. Taking the Laplace transform of the *MSD* and substituting this result into (77) yields $\tilde{G}(s) = \mu s$ giving a complex modulus, $G(\omega) = i\mu\omega$. Consequently, $G'(\omega) = 0$ and $G''(\omega) = \mu\omega$, the real and imaginary parts of *G*, respectively. For a linear elastic (Hookean) solid, $MSD = k_BT / \pi G_0 a$ where G_0 is the constant shear modulus of the material, so that $G'(\omega) = G_0$ and $G''(\omega) = 0$.

In the more general case, but still in keeping with the assumptions given above, the complex shear modulus can be written in the form:

$$\tilde{G}(i\omega) = G^*(\omega) = G' + iG'' = \left|G^*(\omega)\right| \exp(i\delta(\omega)) \tag{78}$$

where $\delta = \arctan[G''(\omega)/G'(\omega)]$, $\left|G^*(\omega)\right|$ is computed from the *MSD* using the approximation (Tschoegl, 1989, Mason et al., 1997):

$$\left|G^*(\omega)\right| \approx \frac{2k_BT}{3\pi a \left\langle \Delta R^2(\tau) \right\rangle \Gamma\left(1 + \dfrac{d\ln\left\langle \Delta R^2(\tau) \right\rangle}{d\ln\tau}\right)} \tag{79}$$

where Γ is the gamma function. The phase angle $\delta(\omega)$ can be obtained from $\left|G^*(\omega)\right|$ using the approximation (Booij and Thoone, 1982):

$$\delta(\omega) \approx \frac{\pi}{2}\left(\frac{d\ln\left|G^*(\omega)\right|}{d\ln\omega}\right) \tag{80}$$

since the storage and loss moduli are related and can be derived from one another provided the complete spectral dependence of one (or a substantial part of it) is known (Ferry, pp. 72-74, 1970).

Measurement Comparisons

Despite (or perhaps because of) the existence of so many methods of measuring the elastic properties of cells, there is considerable debate concerning actual values for the various parameters. The shear modulus, for example, varies over quite a wide range (four orders of magnitude!) as shown in Table 4. While some of this variability no doubt reflects actual differences due to cell type, much is likely also due to inconsistencies either in the assumptions used to interpret the experimental data or the extent to which the biological state of the cells was influenced by the testing procedure. With respect to modeling assumptions, there is currently little agreement concerning the most valid approach. Factors that need to be considered include the following:

- the relative importance of the lipid bilayer, the cortex, the nucleus and the cytoskeleton,
- the size of the probe used to make measurements,
- the extent to which the cytoplasm can be treated as homogeneous,
- the role of adhesion or other biological responses in the vicinity of the probe.

Cell type	*Measurement method*	*Shear modulus (Pa)*	*Reference*
lymphocyte	poking	300	Zahalak et al.
lymphocyte (activated)	poking	700 - 1100	Zahalak et al.
neutrophil (activated)	poking		Zahalak et al.
neutrophil	poking	110	Zahalak et al.
NIH 3T3 fibrobalst	magnetic tweezers	20,000-40,000	Bausch et al.
NIH 3T3 fibroblast	AFM	4,000-100,000	Haga et al.
J774 mouse macrophage	magnetic tweezers	343	Bausch et al.
3T3 and NRK fibroblast	AFM	1,000-10,000	Rotsch & Rademacher
mouse fibroblast	poking	1600 (E)	Peterson et al.
endothelial cell	aspiration	40-50	Theret et al.
bovine endothelial cell	indentation	400-600	Sato et al.
porcine endothelial cell	aspiration	75 (E)	Sato et al.
endothelial cell	magnetic twisting cytometry (MTC)	2.2 (round) (E) 4.5 (spread) (E)	Wang et al.

bovine endothelial cell	MTC	3-7.5	Wang & Stamenovic
human chondrocytes	aspiration	330	Trickey et al.
smooth muscle cell	MTC	11.5 (E)	Stamenovic & Coughlin
COS7 (kidney epithelial)	laser tracking microrheology	33-82 ($\left\|G^*\right\|$)	Yamada, et al.

Table 4. Some representative values for the shear modulus of different cell types. In most cases, these represent the modulus exhibited at long times.

These factors, and many others, will need to be better understood before reliable and consistent measurements can be made.

Micro-structural models

Up to this point, our discussions have been based on the assumption that whatever the structure of the cytoskeleton at the microscale, its mechanical properties as measured or as observed at the scale of a cell can be described in terms of a continuum. This is an expeditious approach, and the one used in most of the studies of cytoskeletal properties. But this approach, that essentially ignores the existence of a fine-scale microstructure can, at best, be only a means of describing the behavior of the actual filamentous network that comprises the cytoskeleton and provides little by way of fundamental understanding the origin of these properties. To gain a full appreciation of how the various constituents of the network – actin filaments, intermediate filaments and microtubules – contribute to the observed properties, one must look, and think, on a much finer scale and consider how the individual filaments contribute to the overall elastic characteristics of the material. It should be obvious that the following microstructural models are just that – models built upon certain assumptions about the mechanical behavior of the cytoskeleton. The fact that several exist, giving quantitatively and even qualitatively different predictions, should suffice to convince the reader that there is no broad consensus as to the validity of any one model, and that they cannot all be valid. Only by the application of experimental methods that probe at the microscale (e.g., laser trap and AFM) will we establish which is appropriate for a given cell type. Several models are presented here mainly because they help to illuminate diverse ways of organizing our thoughts and obtaining testable predictions that will ultimately provide the basis for acceptance or rejection of each.

For the purpose of the present discussion, we will treat the individual filaments as thin elastic fibers made from a homogenous elastic material. (This in itself is a rather broad

assumption as will be seen in the Section on Molecular Mechanics.) These fibers resist axial stretch as characterized by a Young's modulus E_f defined by the following relation between axial stress and strain:

$$\tau_{ii} = E_f \varepsilon_{ii} \tag{31}$$

(summation convention not used) and resist bending as characterized by a bending stiffness $K_b = E_f I$ with I the moment of inertia, defined for small deflections y through,

$$M = E_f I \left(\frac{d^2 w}{dx^2} \right) = K_b \kappa \tag{32}$$

where x is distance measured along the axis of the fiber, w is the fiber deflection, and κ is the curvature, the inverse of the radius of curvature. Eqn. (32) can be derived from the more general relationships obtained in Chapter 1.2 by taking the equation relating stress and strain (Eqn. (9) or (10)) and setting the lateral stresses equal to zero. The Young's modulus of a filament on the scale of F-actin can be shown to be due to two effects that are classified by their thermodynamic basis. The first is the enthalpic contribution and arises from all force interactions. The second is termed the entropic contribution and is related to the probability distribution of possible configurations the molecule might exhibit. These issues are discussed in more detail in Section III in the context of single molecule mechanics. For the present discussion, we will simply assume that the fibers to have some elastic modulus that can be measured.

Some networks derive their structural integrity from an interaction between members that are in compression and members in tension. Some familiar large-scale examples include the circus tents and the geodesic dome. In the case of the circus tent, the rigidity of the structure is due to the balance between the tent poles in compression and the ropes anchored to the ground in tension. A simple demonstration can be constructed from wooden dowels in combination with elastic bands as shown in Fig. 10. In this two-dimensional model, the compression elements are effectively rigid; deformations occur by a rotation of the dowels and a lengthening or shortening of the elastic bands on the horizontally and vertically aligned members, respectively (Fig. 10b). The rigidity of the structure, in this case, is related to the elastic characteristics of the tension elements. Ingber [1998] has proposed that the cytoskeleton behaves like a tensegrity structure with the microtubules acting in compression and the F-actin microfilaments acting in tension. In support of this concept, microtubules have been shown to be capable of supporting compressive loads and the F-actin network exhibits behavior at junctions consistent with their

being in tension. The intermediate filaments may also be involved, although their contributions at this stage are unclear.

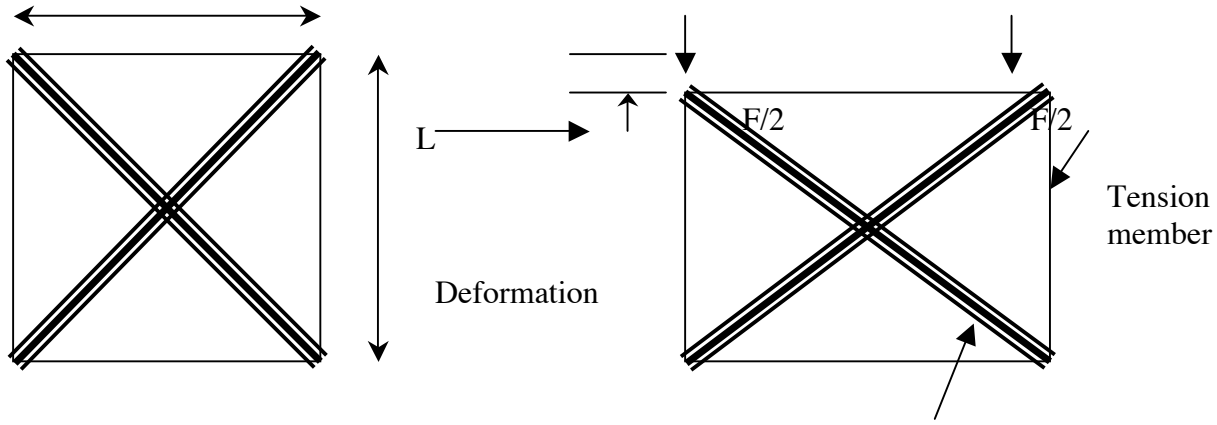

Fig.10. Simple, 2-strut model of a tensegrity structure before (a) and after (b) a small deformation.

Although the description of structures having many members is quite complex, simple structures such as the one in Fig. 10 are more amenable to analysis. Consider the response of the structure shown to the application of vertical forces at the two vertices, each of magnitude *F/2*. The structure deforms a distance δ as a result of a lengthening of the upper and lower tension elements, and a shortening of those on the two sides. In the deformed state, the change in elastic energy must equal the work done by the forces. Noting that the strain in the elastic elements is $\varepsilon = \pm\delta/L$ (for the horizontal (+) and lateral (-) elements), and recalling from Chapter 1.3 that the strain energy density is $\tau\varepsilon/2$, the total strain energy in the deformed state is

$$U \approx \int_0^{L_1} \tau_f \varepsilon_{f1} a^2 \, dx + \int_0^{L_2} \tau_f \varepsilon_{f2} a^2 \, dx \tag{33}$$

where a is the element radius, assumed circular in cross-section, and the strains ε_{f1} and ε_{f2} correspond to the strains in the horizontal and vertical elastic elements, respectively. If we allow for a non-zero initial stress τ_{fo} in the elastic elements (equal in all elements), and assuming each to be linearly elastic with Young's modulus E_f, the change in elastic energy under an additional deformation δ, summed for all four members and subtracted from the initial energy, gives the following result:

$$\Delta U \sim La^2\left(\frac{\delta}{L}\right)^2\left(2\tau_{f0}+E_f\right) \tag{34}$$

Here the two linear contributions from Eq. (33) can be seen to cancel. Equating this to the work done yields

$$F\delta \sim La^2\left(\frac{\delta}{L}\right)^2\left(2\tau_{f0}+E_f\right) \tag{35}$$

If we imagine a three-dimensional structure constructed from a collection of these two-dimensional unit cells, spaced on average a distance L apart (in the direction perpendicular to the plane of the paper in Fig. 10), we can introduce an effective stress within the network, τ_n, estimated to be

$$\tau_n \propto \frac{F}{L^2} \propto \left(2\tau_{f0}+E_f\right)\left(\frac{a}{L}\right)^2\frac{\delta}{L} \tag{36}$$

from which we can compute the following scaling relation for the network Young's modulus

$$E_n \sim \frac{\tau_n}{\delta/L} \propto \left(2\tau_{f0}+E_f\right)\left(\frac{a}{L}\right)^2 \propto \left(2\tau_{f0}+E_f\right)\Phi \tag{37}$$

This result suggests a linear dependence on solid fraction and (if we focus on the first term in parentheses) prestress. It is important to note here, that *the network modulus depends both on the properties of the filaments that make up the network and the network prestress*. This is a unique property of a tensegrity network and distinguishes it from the other models presented in this chapter.

When a more realistic three-dimensional tensegrity network (Fig. 11) is used, analysis again shows that pre-stress plays a dominant role. Intuitively, it is not surprising that networks with greater pre-tension in the elastic members should exhibit greater resistance to deformation. Results for the structure of Fig. 11 are shown in Fig. 12. Here, the effect of pre-stress is seen to increase the network Young's modulus for small strains, and that only in the limit of infinite pre-stress does E_n become independent of pre-stress. Ingber and co-workers [] have shown that the cytoskeleton exhibits this same tendency, becoming increasingly stiff when, for example, the cell passes from a spherical (low pre-stress) to flattened (high pre-stress) state. Other models of cytoskeletal mechanics, however, might also exhibit this *strain-stiffening* behavior.

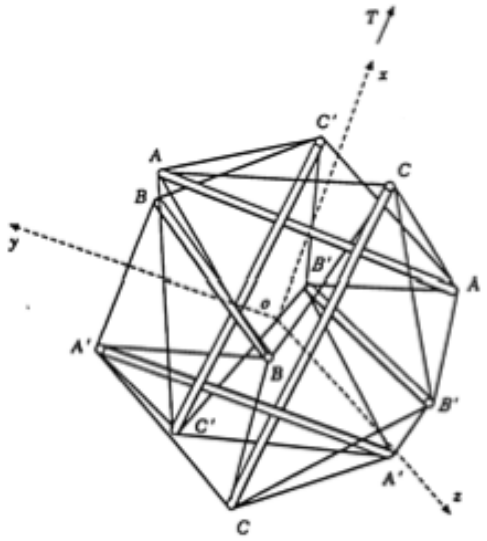

Fig. 11. A three-dimensional, 6-strut model of a tensegrity structure. (Reproduced from Stamenovic et al., 1996)

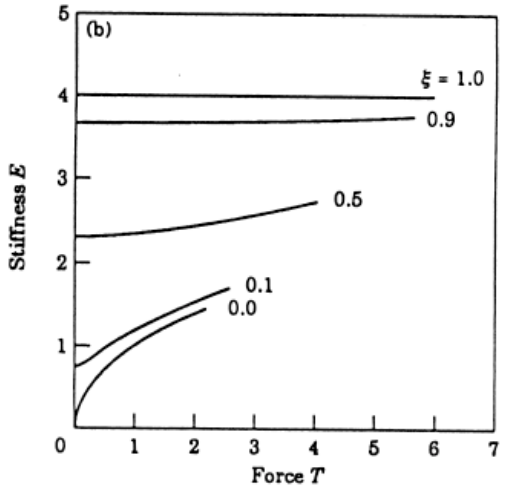

Fig. 12. The predicted response of the structure shown in Fig. 11 when the elastic members are assumed to have a linear elasticity and the compression members are assumed rigid. T is the stretching force and ξ is the level of prestrain in each elastic member. Note that the stiffness, E, increases with increasing prestrain, in roughly a linear manner. (Reproduced from Stamenovic, et al., 1996.)

A potentially significant shortcoming of this model is the complete absence of any influence on elasticity of thermal fluctuations, the importance of which has been manifestly demonstrated in studies of entanglement matrices and gels. Both the tensegrity model and the cellular solids model discussed next omit such effects. They are, however, considered in the models of biopolymer networks discussed later.

Cellular Solids

The theory of cellular solids was developed for the purpose of relating the macro-mechanical properties of low-density cellular materials to their micro-structural characteristics. The approach used is based on the concept that the material can be modeled as being comprised of many "unit cells", one representation of which is shown in Figure 13. These unit cells are staggered with struts meeting at their midpoints. It should be noted that the following analysis, while developed with the structure of Figure 13 in mind is applicable to a variety of fibrous materials with different microstructures and is not restricted to this particular geometry. When a cellular solid is stressed under tension or compression, the fibers act like struts and beams that deform under stress as illustrated in Figure 13b.

The unit cell model in Figure 13 has struts or fiber elements of length L and cross section of radius a. The relative density of the material is defined by the volume fraction of solid material, Φ. This is calculated as the solid volume contained within a unit cell $(\sim a^2 L)$ divided by the total unit cell volume $(\sim L^3)$ or

$$\Phi \sim (a/L)^2 \tag{38}$$

Beam theory, as developed in Chapter 1.2, gives the deflection δ of a beam of length L subject to a force F acting at its midpoint as

$$\delta \sim FL^3/(E_f I) \tag{39}$$

where E_f is the stiffness of the beam constitutive material and I is the beam's second moment of area. The moment of area for a beam of thickness a is given by

$$I \sim a^4 \tag{40}$$

The stress τ is the force per unit area, or

$$\tau \sim F/L^2 \tag{41}$$

The strain is related to beam deflection δ by

$$\varepsilon \sim \delta/L \tag{42}$$

Using the results from eqns. (39), (41), and (42), the network Young's modulus or elastic modulus can be expressed as

$$E_n = \tau/\varepsilon = c_1 E_f I/L^4 \tag{43}$$

where c_1 is a constant of proportionality. Substituting equations (38) and (40) into (43) gives:

$$E_n/E_f = c_1\, \Phi^2 \tag{44}$$

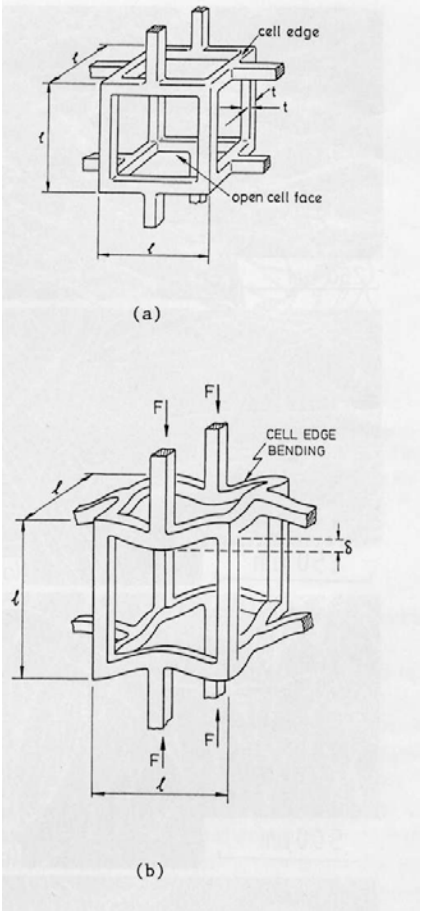

Fig. 13 Unit cell used in the cellular solids model.

Data from a wide range of materials and cell geometries give a value for c_1 of approximately 1 (see Fig. 14). A similar analysis for cellular materials subjected to shear stresses results in an expression for the network shear modulus G_n given by Gibson & Ashby ():

$$G_n/E_f \sim c_2 \Phi^2 \tag{45}$$

where $c_2 \sim 3/8$. If the material is linearly elastic and isotropic, elasticity theory provides the following relationship

$$G_n = E_n/[2(1+\nu)] \tag{46}$$

which, when solved for the Poisson ratio ν, gives a value of 1/3.

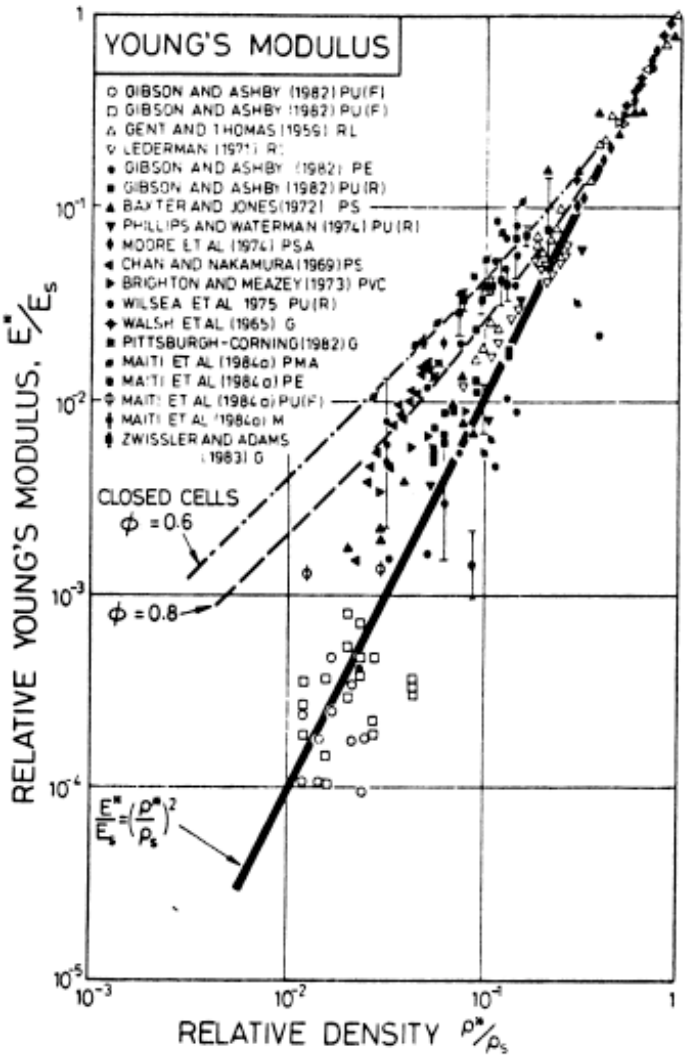

Fig. 14. Plot of the effective Young's modulus various fibrous materials. Gibson & Ashby, 1988.

Biopolymer networks

Cytoskeletal networks can also be viewed as a polymer gel in which the matrix is considered to consist of relatively straight segments connecting junctions where the filaments are either

chemically cross-linked, or effectively so due to entanglements. This picture has some similarity to the one with which we began the cellular solids analysis, but the approach employed from this point on is somewhat different. Using concepts from polymer physics (see e.g., Isambert and Maggs, 1996) the force required to change the length of one segment of a polymer filament (F-actin, for example) of length L_e by an amount δ can be expressed as

$$F_T \approx \frac{k_B T l_p^2}{L_e^4}\delta \approx \frac{K_b^2}{k_B T L_e^4}\delta \tag{47}$$

where k_B is Boltzmann's constant, T is temperature, K_b is the bending stiffness of the filament, l_p is the persistence length, and L_e is the distance between the points where the tension is applied (or, the distance between points of entanglement or cross-linking between network filaments). This expression arises from a consideration of the curvature of the polymer resulting from Brownian or thermal fluctuations, and is based on the assumption that thermal energy is equally partitioned among the different modes of oscillation. The polymer filaments are therefore assumed to be bent prior to the application of stress. Externally-imposed forces either increase or decrease the end-to-end length of these filaments, and the deformation produced depends both on the intrinsic bending stiffness of the filaments and on their initial degree of curvature due to thermal fluctuations. This can immediately be seen to differ from the approach in the cellular solids model where the filaments are viewed as initially straight, lacking any significant thermally-induced motions, with the imposed stresses causing filament bending.

For a network comprised of such filaments in which the distance separating points at which physical bonds exist between the filaments or regions of entanglement is L_e, the change in filament length between bonds due to a shear strain θ (see Fig. 15) is

$$\delta \sim \theta L_e \tag{48}$$

Making use of the fact that the number of filaments per unit area parallel to the surface on which the stress is applied scales inversely as the square of the characteristic mesh spacing ξ, the shear stress required to produce a strain θ is given by eqns. (47) and (48):

$$\tau \sim F_T \cdot (number\ of\ filaments)/(unit\ area) \sim k_B T l_p{}^2 \theta/(L_e{}^3 \xi^2) \tag{49}$$

from which a shear modulus of the network G_n can be determined as the ratio of stress to strain

$$G_n \sim \tau/\theta \sim k_B T l_p{}^2/(L_e{}^3 \xi^2) \tag{50}$$

The scaling of G_n clearly depends on both the distance between cross-links or entanglements and the mesh size. As the concentration of polymer increases, ξ decreases and so likely does L_e, at least in terms of the degree of entanglement. As the concentration of actin binding protein (APB) increases, L_e will decrease.

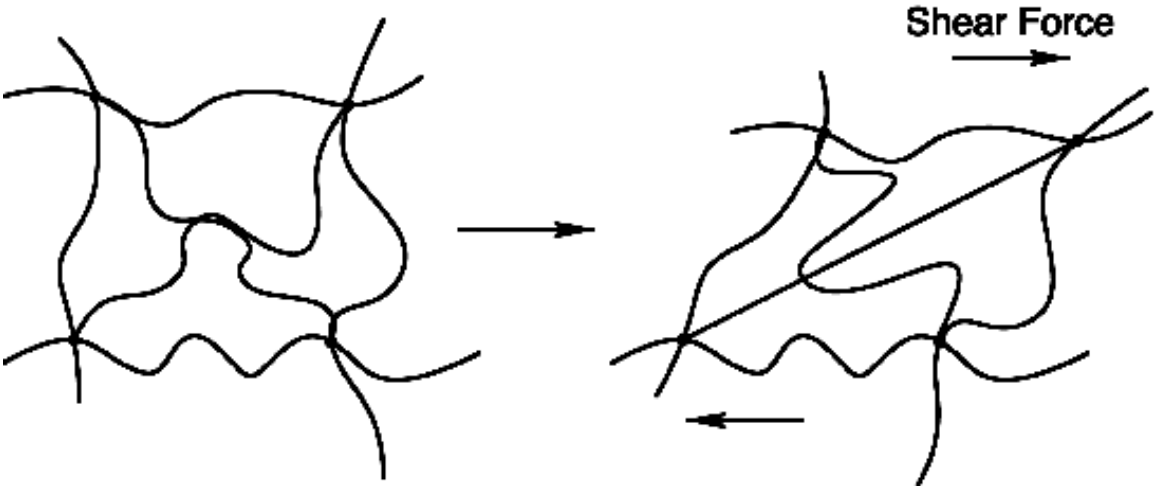

Fig. 15. A fibrous matrix being subjected to a shearing force.

The mesh spacing ξ also depends on the monomer concentration or solid fraction Φ (monomer volume / total volume). Assuming the filaments are stiff and homogeneously dispersed through the medium, this relationship can be expressed as

$$\Phi \sim (\xi a^2)/\xi^3 \tag{51}$$

or

$$\xi \sim a/\Phi^{1/2} \tag{52}$$

where a is the monomer or filaments radius. Substituting above yields

$$G_n \sim k_B T l_p{}^2 \Phi/(L_e{}^3 a^2) \tag{53}$$

In the limit of a highly cross-linked network in which case $L_e \sim \xi$, this leads to

$$G_n \sim k_B T l_p^{-2} \cdot (\Phi/a^2)^{5/2} \tag{54}$$

Here we see a slightly stronger dependence on volume fraction (to the 5/2 power) than exhibited by any of the previous models. Alternatively, we can express this in terms of the density of cross-links, ρ_c. Note that if ρ_c is the number of cross-links per unit volume, it should vary inversely with the volume associated with each bond or entanglement, i.e., as L_e^{-3}. Combining this with eqns. (52) and (53) above:

$$G_n \sim k_B T l_p^{-2} \Phi \rho_c / a^2 \tag{55}$$

The Young's modulus of the network E_n can be obtained by a similar procedure, and can be shown to scale in the same manner as G_n.

Equation (55) is an interesting result, and provides an opportunity to see how the addition of some agent such as ABP can affect cytoskeletal strength. Assuming the amount of polymer remains fixed, and only the degree of cross-linking changes, the change in modulus should be linear in ρ_c. This is a speculative result at this stage, and needs to be tested by experiment.

2.2.5 Fluid properties of the cytosol

So far, our discussion has focused on the protein filaments that comprise the cytoskeletal matrix within the cell, how to measure its characteristics and how it has been modeled. This matrix, however, is immersed in fluid, the cytosol, and the dynamic response of the cell is influenced by the properties of this fluid. The properties that one measures, however, depend upon how the measurement is made as illustrated in the following examples.

Several methods have been used to infer the viscosity of the cytosol, but here we focus on two: micropipet aspiration and dynamic light scattering. When a cell is aspirated into a micropipet under a sufficiently large suction pressure that it continues to flow into the pipette, the rate at which it enters can be used to determine the cytosolic viscosity. The model of the neutrophil used in these studies is that of a viscous droplet encapsulated in a thin shell that behaves as though it was in a state of constant tension (of about 3.3×10^{-5} N/m) (see also Chapter 2.4). Using this model, several investigators obtained values for cytosolic viscosity that vary widely from about 10-30 Pa·s (Dong, et al., 1988) all the way up to about 200 Pa·s (Evans & Yeung, 1989, Needham & Hochmuth, 1990), all for the same cell type, neutrophils.

Tsai et al, 1993, were able to reconcile some of these differences by assuming the cytoskeleton to behave as a *power-law fluid*, that is, one in which viscosity behaves according to the expression

$$\mu = \mu_c \left(\frac{\dot{\gamma}_m}{\dot{\gamma}_c} \right)^{-b} \tag{81}$$

where μ_c is the viscosity at a shear rate of $\dot{\gamma}_c$ and b is a constant determined from the experiments. For passive neutrophils, they found the following values from seven different experiments: μ_c = 130 +-23 Pa·s for $\dot{\gamma}_c$ =1 s^{-1} and b = 0.52+-0.09.

These measurements with micropipet aspiration can be contrasted with measurements made by analysis of the rotations of polarized molecules introduced into the cell (Fushimi and Verkman, 1998) that yield a value for viscosity very near that of water, about 1.2-1.4 $x10^{-3}$ Pa·s. This discrepancy of roughly five orders of magnitude can be reconciled on the basis of differences in scale of the two measurement probes. When the neutrophil is drawn into the micropipet, all of the cytoplasmic structures and macromolecular constituents are being caused to flow and affect the measured viscosity. With the high concentration of large molecular weight species that are present, it is hardly surprising that the fluid exhibits a high viscosity and non-Newtonian characteristics. Dynamic light scattering methods, by contrast, probe the fluid phase only. Effectively, the scale of measurement is microns in the aspiration method and nanometers in the light scattering method. Which value for the viscosity one should use in any given situation must be dictated by the nature of the problem of interest. To estimate the viscous interaction between the cytoskeleton and the cytosol flowing past it, the fluid should be assumed to behave essentially like water. To estimate the viscous response of the cell to being squeezed between two flat surfaces, the higher value corresponding to the entire collection of constituents must be used.

3.2.7 Nomenclature:

a - radius
ε_{ij} – infinitesimal strain tensor
e_{ij} – finite amplitude strain tensor
E – Young's modulus (Pa)
E – Strain energy (Nm)
F - force (N)
G – Shear modulus (Pa)
k – spring constant (N/m)
k_B – Boltzmann's constant
K_b – bending stiffness (N·m)
L – Length of filament (m)
T - temperature (K)
u - displacement (m)
τ_{ij} - stress tensor (Pa)
δ - deflection during a deformation test (m)
μ - damping constant (Ns/m)
ν – Poisson's ratio
η - effective viscosity of a viscoelastic solid ()
ξ - filament spacing (m)
Φ - filament solid fraction
Θ - torque (Nm)
C – concentration (kg/m^3)
Δp - pressure applied in micropipette aspiration (Pa)

Subscripts:
n – network
f – filaments
0 – initial response
∞ - long time or steady-state response

References (partial list)

1. Hall, A, Rho GTPases and the actin cytoskeleton. *Science*, 27: 509-514 , 1998.

2. Yeung, A and Evans, E. Cortical shell-liquid model for passive flow of liquid-like spherical cells into micropipets. *Biophysical Journal*, 56:139-149, 1989.

3. Satcher, R, Dewey, CF, Jr. and Hartwig, JH. Mechanical Remolding of the Endothelial Surface and Actin Cytoskeleton Induced by fluid flow. *Microcirculation*, 4(4):439-453, 1997.

4. Zahalak, GI, McConnaughey, WB. and Elson, EL. Determination of Cellular Mechanical Properties by Cell Poking, With an Application to Leukocytes. *Journal of Biomechanical Engineering*. 112:283-294, 1990

5. Zhelev, DV, Needham, D, and Hochmuth, RM. A Novel Micropipet Method for Measuring the Bending Modulus of Vesicle Membranes, *Biophysical Journal*, 67:720-727, 1994.

6. Stamenovic, D, Fredberg, JJ, Wang, N, Butler, JP and Ingber, DE. A Microstructural Approach to Cytoskeletal Mechanics based on Tensegrity, *J. Theor. Biol*. (1996) 181:125-136.

7. Zhelev, DV, Needham, D and Hochmuth, M. A novel micropipet method for measuring the bending modulus of vesicle membranes. *Biophys. J*., 67:720-727, 1994.

8. Choquet, D, Felsenfeld, DP and Sheetz, MP. Extracellular Matrix Rigidity Causes Strengthening of Integrin-Cytoskelton Linkages, *Cell*,. 88:39-48, 1997.

9. Haga, H, Sasaki, S, Kawabata, K, Ito, E, Ushiki, T, Sambongi, T. Elasticity mapping of living fibroblasts by AFM and immunolfuorescence observation of the cytoskeleton. Ultramicroscopy 82:253-258, 2000.

10. Vegners, R, Shestakova, I, Kalvinish, I, Ezzell, RM, and Janmey, PA. Use of a gel-forming dipeptide derivative as a carrier for antigen presentation. *J. Peptide Science*, 1:371-378, 1995.

11. Theret, DP, Levesque, MJ, Sato, M, Nerem, RM, and Wheeler, LT. The application of a homogeneous half-space model in the analysis of endothelial cell micropipette measurements. *J. Biomech. Engineering*, 110:190-199, 1988.

12. Fuchs, E and Cleveland, DW. A structural scaffolding of intermediate filaments in health and disease. *Science*, 27: 514-519, 1998.

13. Zhelev, DV, Needham, D and Hochmuth, M. Role of the membrane cortex in neutrophil deformation in small pipets. *Biophys. J.*, 67:696-705, 1994.

14. Evans, E and Yeung, A. Apparent viscosity and cortical tension of blood granulocytes determined by micropipet aspiration. *Biophysical Journal*, 56:151-160, 1989.

15. Ingber, DE. The architecture of life. *Scientific American*, pp. 48-57, January, 1998.

16. Janmey, PA. Mechanical properties of cytoskeletal polymers. *Current Opinion in Cell Biology*, 2:4-11, 1991.

17. MacKintosh, FC and Janmey, PA. Actin gels. *Current Opinion in Solid State & Materials Science*, 2:350-357, 1997.

18. Satcher, RL, Jr. and Dewey, CF, Jr. Theoretical estimates of mechanical properties of the endothelial cell cytoskeleton. *Biophys. J.*, 71:109-118, 1996.

19. Johnson, K.L. *Contact Mechanics*. Cambridge University Press, Cambridge. p. 452, 1985.

20. Gibson, LC and Ashby, MF, *Cellular Solids: Structure and Properties*. Pergamon Press, Oxford 1988.

21. Gittes FB, Mickey J, Nettleton J, and Howard J, Flexural rigidity of microtubules and actin filaments measured from thermal fluctuations in shape. J Cell Biol 120:923-934, 1993.

22. Fushimi K, Verkman AS Low viscosity in the aqueous domain of cell cytoplasm measured by picosecond polarization microfluorimetry, Cell Biol 1991 Feb;112(4):719-725.

23. Boulbitch, AA Strain of a biomembrane caused by a local tangential force: Application to magnetic tweezer measurements, Phy Rev E, 59:3402-3407, 1999.

24. Ferry, JD Viscoelastic Properties of Polymers, John Wiley & Sons, New York, 1970.

25. Isambert H, Maggs AC Dynamics and rheology of actin solutions, Macromolecules, 29:1036-1040, 1996.

26. Pine DJ, Weitz DA, Chaikin PM, Herbolzheimer E Diffusing-wave spectroscopy. Phys Rev Lett, 60(12):1134-1137, 1988.

27. Palmer A, Mason TG, Xu J, Kuo SC, Wirtz D Diffusing wave spectroscopy microrheology of actin filament networks. Biophys J, 76:1063-1071, 1999.

20.310J / 3.053J / 6.024J / 2.797J Molecular, Cellular, and Tissue Biomechanics
Spring 2015